Supporting information

Exploring a series of multifunctional Mn(I) tricarbonyls as prospective agents against trypanosomatid parasites: a comparative study with the Re(I) analogues

Carolina Del Mármol,[1,2,3] Gonzalo Scalese,[1] Rodrigo Moreira,[1,2,3] Nicolás Veiga,[1] Ignacio Machado,[4] Ricardo Faccio,[5] Analía Lima,[6,7] Rosely Peralta,[8] Leticia Pérez-Díaz,[9] Dinorah Gambino*[1]

[1] Área Química Inorgánica, DEC, Facultad de Química, Universidad de la República, Uruguay
[2] Programa de Posgrado de Facultad de Química, Universidad de la República, Uruguay
[3] PEDECIBA - Programa de Desarrollo de las Ciencias Básicas, Uruguay
[4] Área Química Analítica, DEC, Facultad de Química, Universidad de la República, Uruguay
[5] Área Física, DETEMA, Facultad de Química, Universidad de la República, Uruguay
[6] Unidad de Bioquímica y Proteómica Analíticas, Institut Pasteur de Montevideo, Uruguay
[7] Instituto de Investigaciones Biológicas Clemente Estable, Uruguay
[8] Departamento de Química, Universidade Federal de Santa Catarina, Florianópolis, Brazil
[9] Sección Genómica Funcional, Facultad de Ciencias, Universidad de la República, Uruguay

E-mail: dgambino@fq.edu.uy; Fax: +5982-9241906; Tel: +5982-9249739

Computational methods

DFT-based quantum chemical methods were used to estimate the water–octanol partition coefficients (log*P*) of the coordination compounds, according to the following process:

$[\mathbf{M}(CO)_3(CTZ)(NN)]^+(ac) + PF_6^-(ac) \rightleftharpoons [\mathbf{M}(CO)_3(CTZ)(NN)]^+(oct) + PF_6^-(oct)$

where M = Re(I) or Mn(I), and NN = phen, bipy, dmb, tmp or aminophen.

To do so, the geometries of the species involved were optimized in solution, and the absolute free energy values were employed in the following equation:

$$logP = log\left(e^{-\frac{G_{n-Octanol} - G_{water}}{RT}}\right) \quad \text{Eq. 1}$$

where *G (Gibbs free energy)* is expressed in kcal/mol, R = 0.001987 kcal/molK and T = 298.15 K. All the calculations were performed using the Gaussian 16 program,[1] and the nature of the stationary points was verified through vibrational analysis.
Firstly, we selected the *fac*-$[Re(CO)_3(CTZ)(phen)](PF_6)$ compound, for which the crystalline structure (used as a reliable input geometry for the optimization step) and experimental log*P* were known. The log*P* was then computed using the SMD continuum solvation model, in conjunction with a combination of six different functionals (B3LYP [2], B3PW91 [3], M06L [4], O3LYP [5], ωB97XD [6] and PBE0 [7]) and four basis sets (LANL2DZ [8], Def2SVP [9], LANL2DZ (Re)/6-31G**(C, N, O, P, F, H) and Def2SVP (Re)/6-31G**(C, N, O, P, F, H) [10,11]).
The best-performing functionals (B3LYP, M06L, ωB97XD and PBE0) and basis set (LANL2DZ) were then employed to calculate the log*P* values for the rest of the Re(I) complexes. The results across the Re(I) systems allowed us to identify the top-performing levels of theory, M06L/LANL2DZ and ωB97XD/LANL2DZ, which were subsequently applied to the Mn(I) tricarbonyl complexes.
The SMD implicit solvation model was used throughout the computational analysis. Additionally, the SMD solvation model was employed for the aminophen-containing complexes, incorporating two hydration water molecules positioned to simulate hydrogen bond interactions with the $-NH_2$ group. The geometries of aminophen-containing complexes with one, two, and three water molecules were optimized. No energy minima were found with three water molecules. With two water molecules, higher log*P* values were obtained, which were closer to the experimentally observed values. This adjustment was essential to achieve computational results that closely matched the experimental log*P* values.
The net atomic charge (NAC) and corrected molecular dipole were calculated employing the Density Derived Electrostatic and Chemical atomic population analysis (DDEC6), as implemented in the Chargemol program. [12] The molecular polarity index (MPI) and nonpolar surface area were calculated using Multiwfn software. [13] All surfaces were modeled using ChemCraft software. [14]

References

1. Frisch, M.J.; Trucks, G.W.; Schlegel, H.B.; Scuseria, G.E.; Robb, M.A.; Cheeseman, J.R.; Scalmani, G.; Barone, V.; Petersson, G.A.; Nakatsuji, H.; et al. Gaussian 16, Revision C.01 2019.

2. Becke, A.D. Density-functional Thermochemistry. III. The Role of Exact Exchange. *J Chem Phys* 1993, **98**, 5648–5652, doi:10.1063/1.464913.

3. Perdew, J.P.; Wang, Y. Accurate and Simple Analytic Representation of the Electron-Gas Correlation Energy. *Physical Rwview B* 1992, **45**, 13244–13249.

4. Zhao, Y.; Truhlar, D.G. The M06 Suite of Density Functionals for Main Group Thermochemistry, Thermochemical Kinetics, Noncovalent Interactions, Excited States, and Transition Elements: Two New Functionals and Systematic Testing of Four M06-Class Functionals and 12 Other Functionals. *Theor Chem Acc* 2008, **120**, 215–241, doi:10.1007/s00214-007-0310-x.

5. Cohen, A.J.; Handy, N.C. Dynamic Correlation. *Mol Phys* 2001, **99**, 607–615, doi:10.1080/00268970010023435.

6. Chai, J.-D.; Head-Gordon, M. Long-Range Corrected Hybrid Density Functionals with Damped Atom–Atom Dispersion Corrections. *Phys. Chem. Chem. Phys.* 2008, **10**, 6615–6620, doi:10.1039/B810189B.

7. Adamo, C.; Barone, V. Toward Reliable Density Functional Methods without Adjustable Parameters: The PBE0 Model. *J Chem Phys* 1999, **110**, 6158–6170, doi:10.1063/1.478522.

8. Wadt, W.R.; Hay, P.J. Ab Initio Effective Core Potentials for Molecular Calculations. Potentials for Main Group Elements Na to Bi. *J Chem Phys* 1985, **82**, 284–298, doi:10.1063/1.448800.

9. Weigend, F.; Ahlrichs, R. Balanced Basis Sets of Split Valence, Triple Zeta Valence and Quadruple Zeta Valence Quality for H to Rn: Design and Assessment of Accuracy. *Phys. Chem. Chem. Phys.* 2005, **7**, 3297–3305, doi:10.1039/B508541A.

10. Hehre, W.J.; Ditchfield, R.; Pople, J.A. Self—Consistent Molecular Orbital Methods. XII. Further Extensions of Gaussian—Type Basis Sets for Use in Molecular Orbital Studies of Organic Molecules. *J Chem Phys* 1972, **56**, 2257–2261, doi:10.1063/1.1677527.

11. Hariharan, P.C.; Pople, J.A. The Influence of Polarization Functions on Molecular Orbital Hydrogenation Energies. *Theor Chim Acta* 1973, **28**, 213–222, doi:10.1007/BF00533485.

12. Manz, T.A.; Gabaldon Limas, N.; Sholl, David.S. Chargemol - Program Computing DDEC Atomic Charges Files 2017.

13. Lu, T.; Chen, F. Multiwfn: A Multifunctional Wavefunction Analyzer. *J Comput Chem* 2012, **33**, 580–592, doi:https://doi.org/10.1002/jcc.22885.

14. Andrienko, G.A.; Senchenya, I.N.; Romanov, A. Chemcraft - Graphical Software for Visualization of Quantum Chemistry Computations.

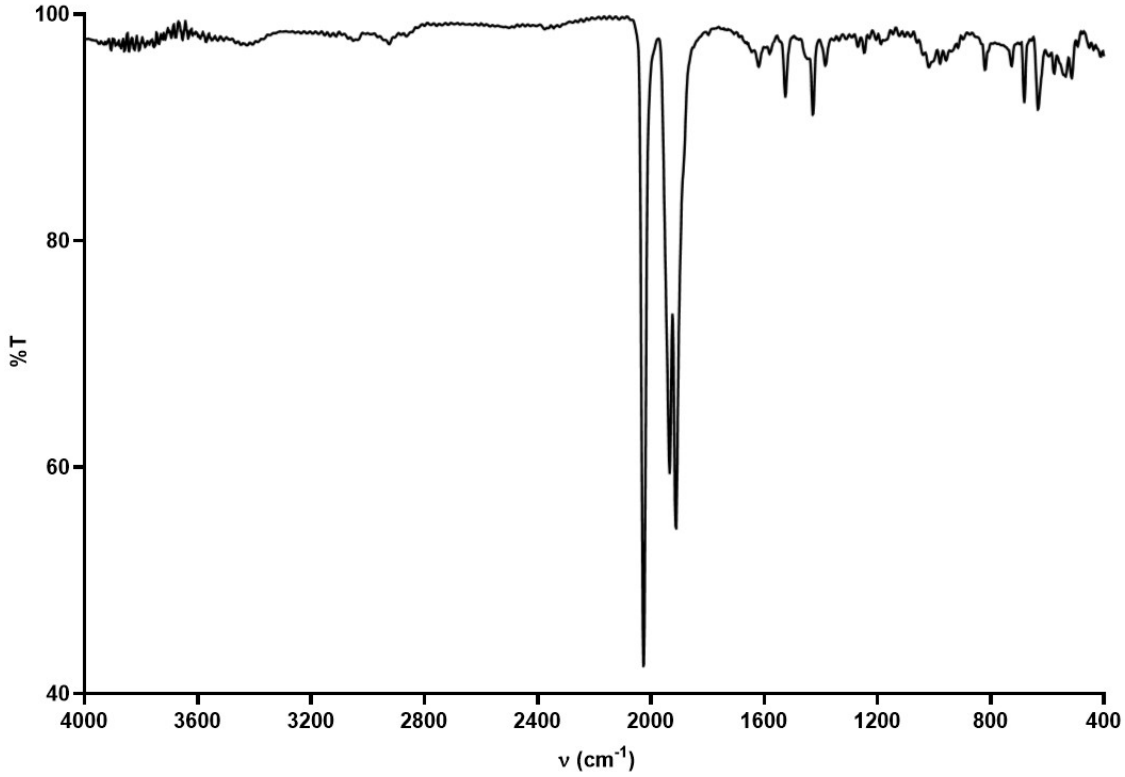

Fig. S1. FTIR spectrum of *fac*-[$MnBr(CO)_3(tmp)$](PF_6), KBr pellets.

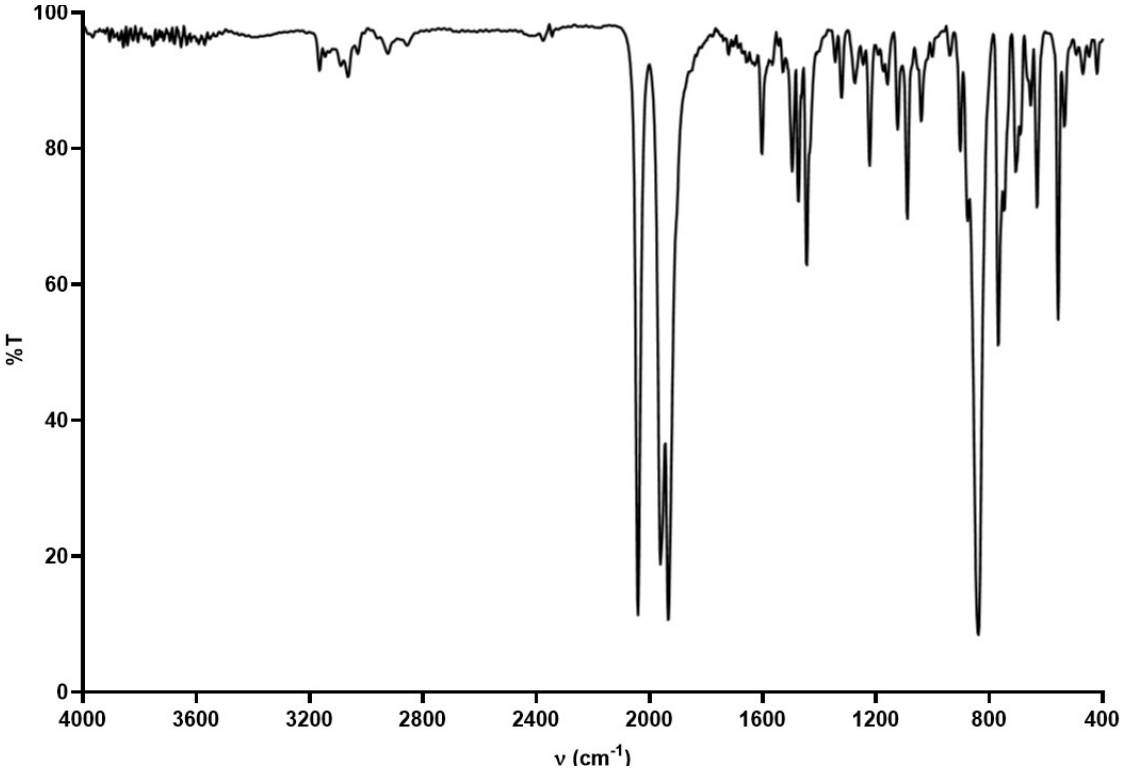

Fig. S2. FTIR spectrum of *fac*-[$Mn(CO)_3(CTZ)(bipy)$](PF_6). KBr pellets.

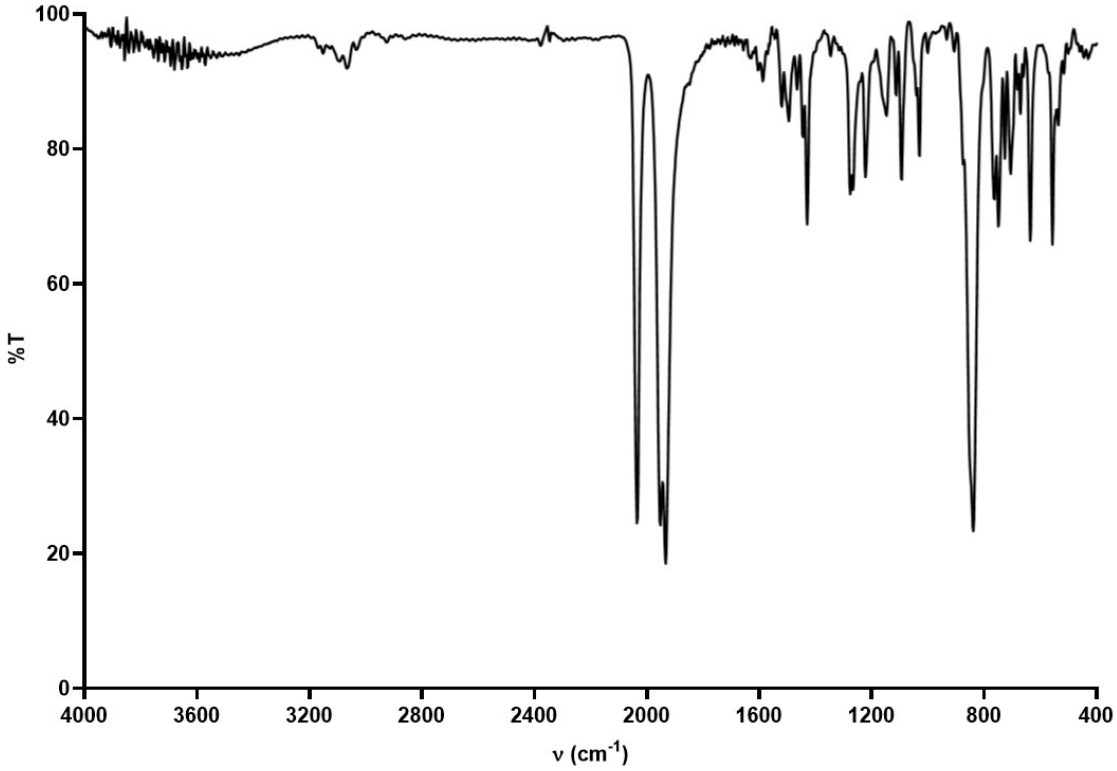

Fig. S3. FTIR spectrum of *fac*-[$Mn(CO)_3$(CTZ)(phen)](PF_6). KBr pellets.

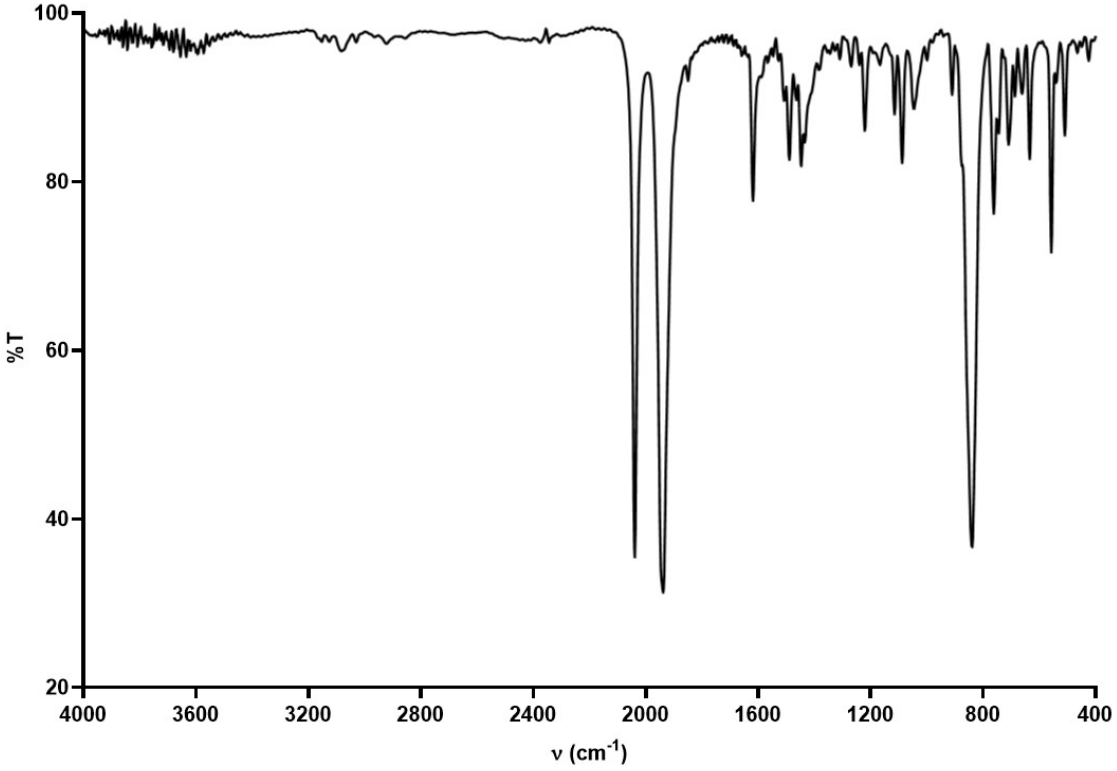

Fig. S4. FTIR spectrum of *fac*-[$Mn(CO)_3$(CTZ)(dmb)](PF_6). KBr pellets.

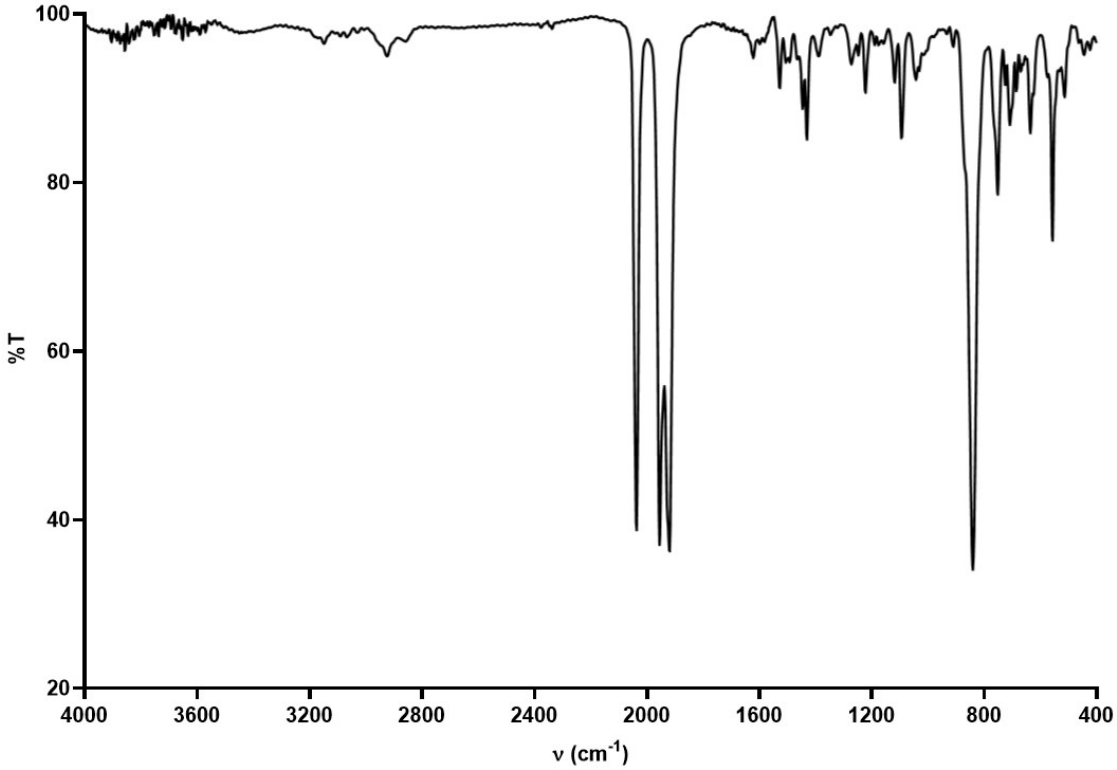

Fig. S5. FTIR spectrum of *fac*-[$Mn(CO)_3$(CTZ)(tmp)](PF_6). KBr pellets.

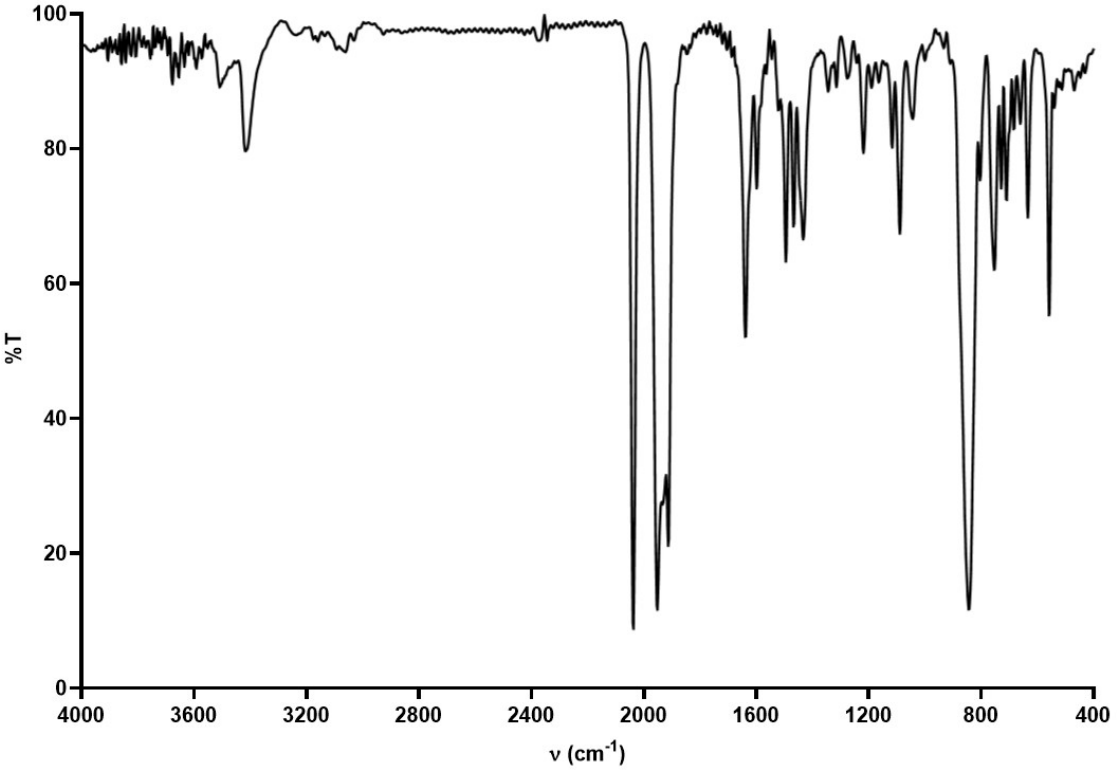

Fig. S6. FTIR spectrum of *fac*-[$Mn(CO)_3$(CTZ)(aminophen)](PF_6). KBr pellets.

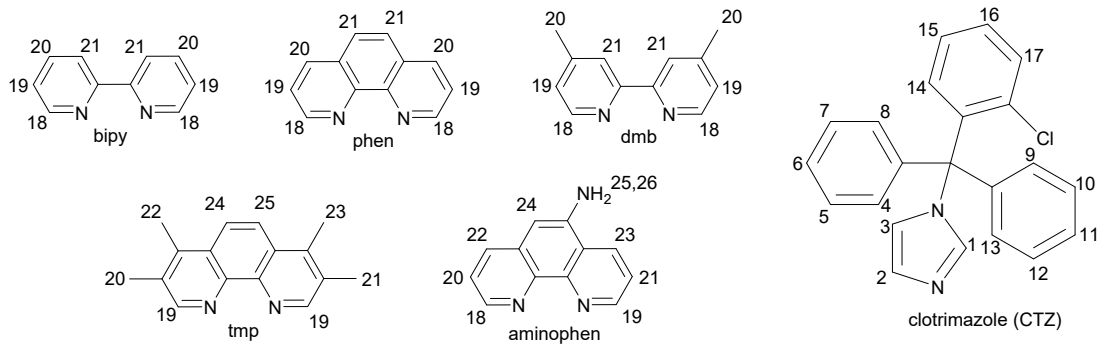

Fig. S7. Numbering scheme of the ligands for ^{1}H-NMR assignment.

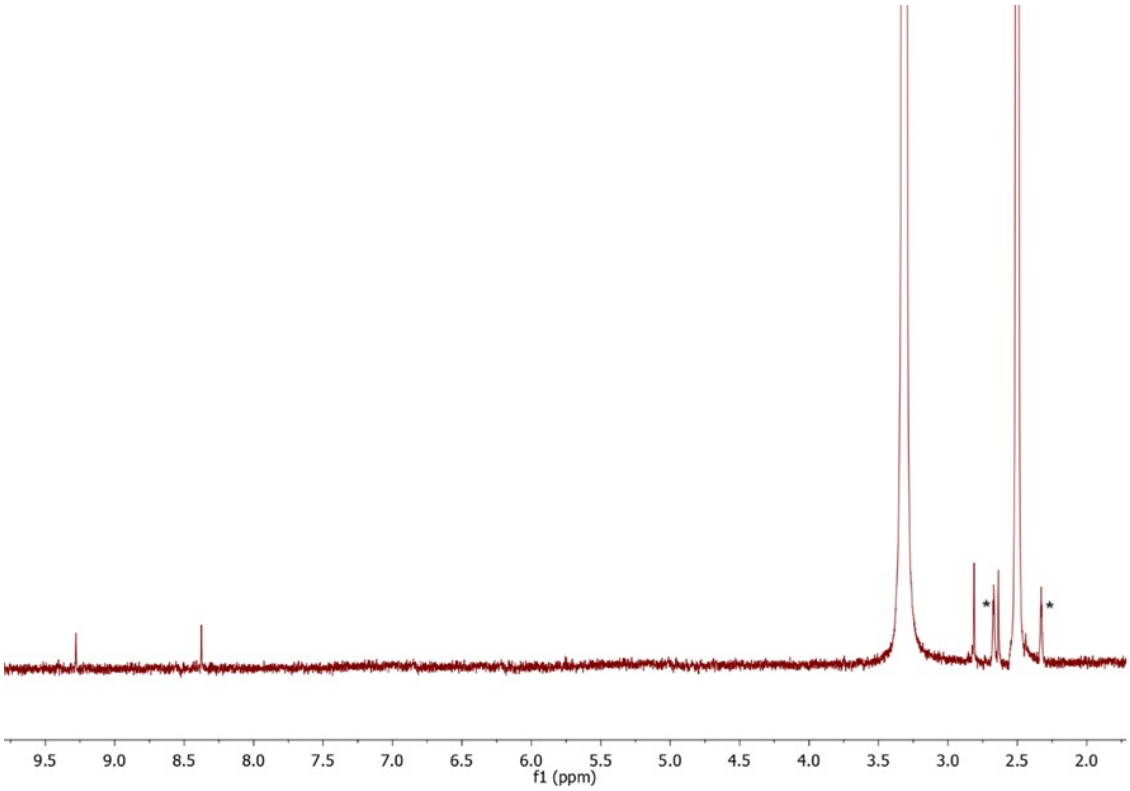

Figure S8. ^{1}H-NMR spectra of *fac*-[MnBr(CO)$_3$(tmp)], DMSO-d$_6$ solution. Signals marked with * are residual DMSO satellite signals. Due to the low solubility of the compound, its signals appear at a similar intensity than DMSO satellite signals.

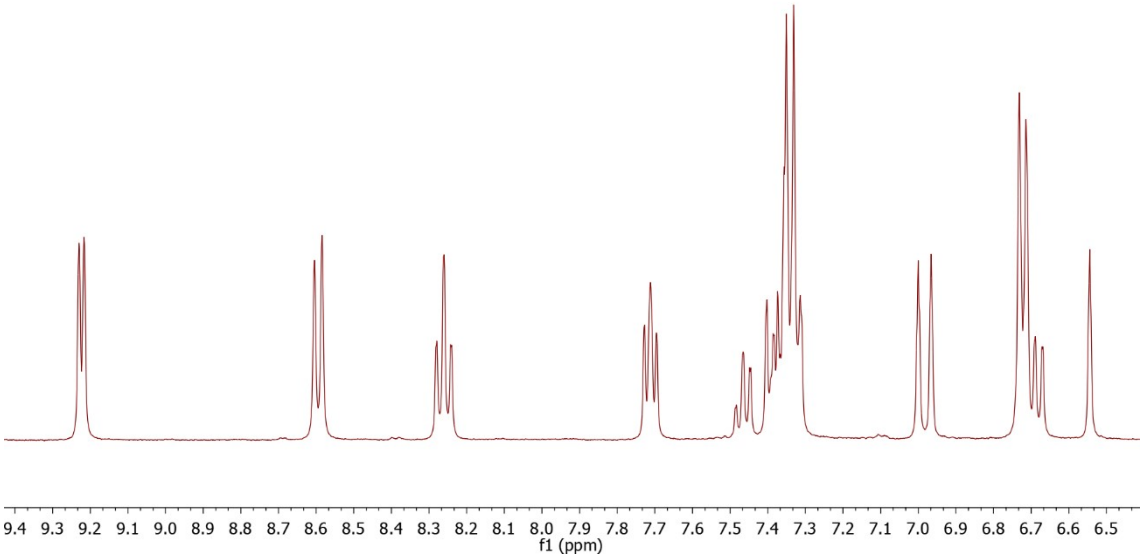

Fig. S9. ^{1}H-NMR spectrum of *fac*-[Mn(CO)$_3$(CTZ)(bipy)](PF$_6$), DMSO-d$_6$ solution.

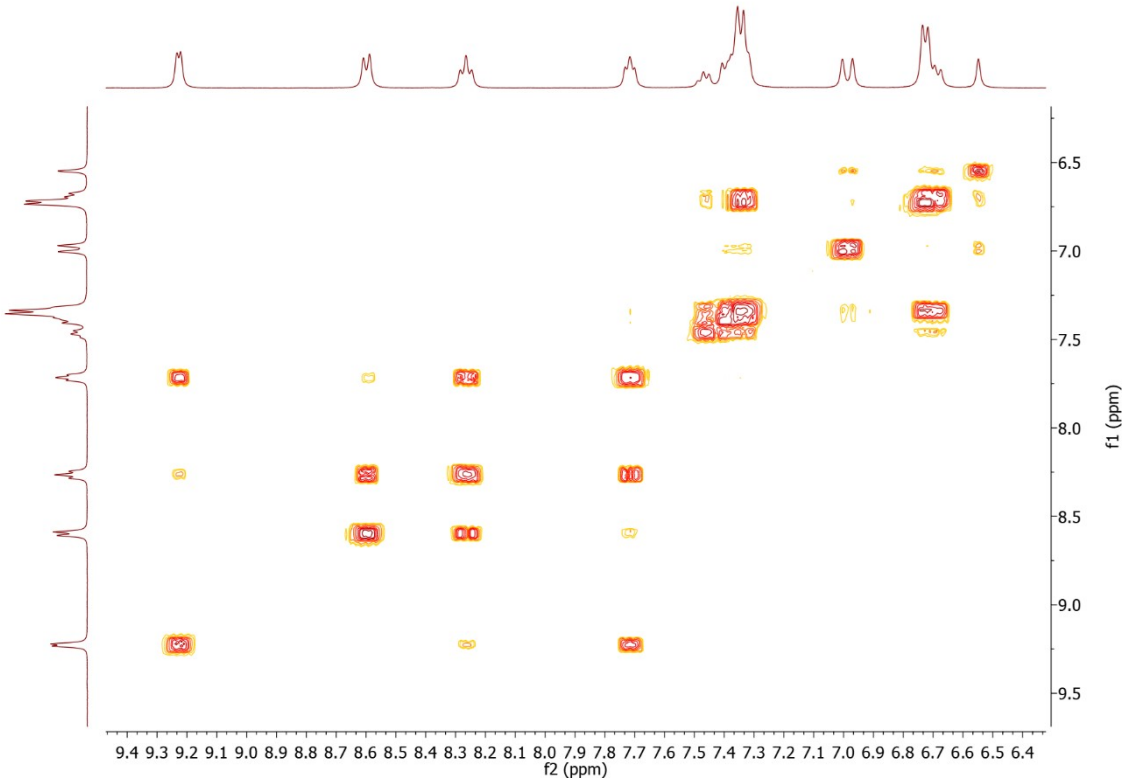

Fig. S10. ^{1}H-^{1}H-NMR (COSY) spectrum of *fac*-[Mn(CO)$_3$(CTZ)(bipy)](PF$_6$), DMSO-d$_6$ solution.

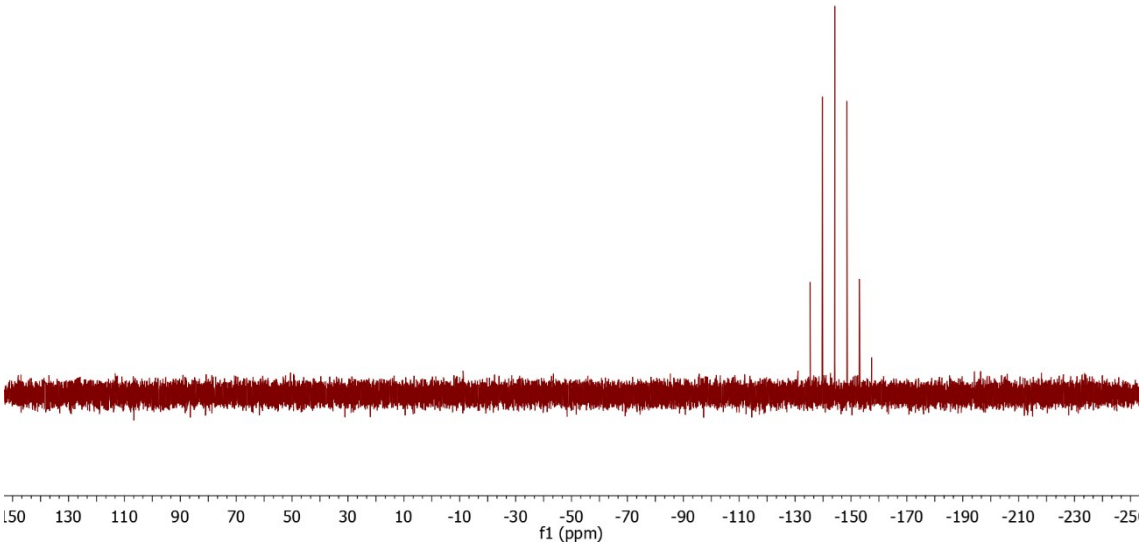

Fig. S11. ^{31}P-NMR spectrum of *fac*-[Mn(CO)$_3$(CTZ)(bipy)](PF$_6$), DMSO-d$_6$ solution.

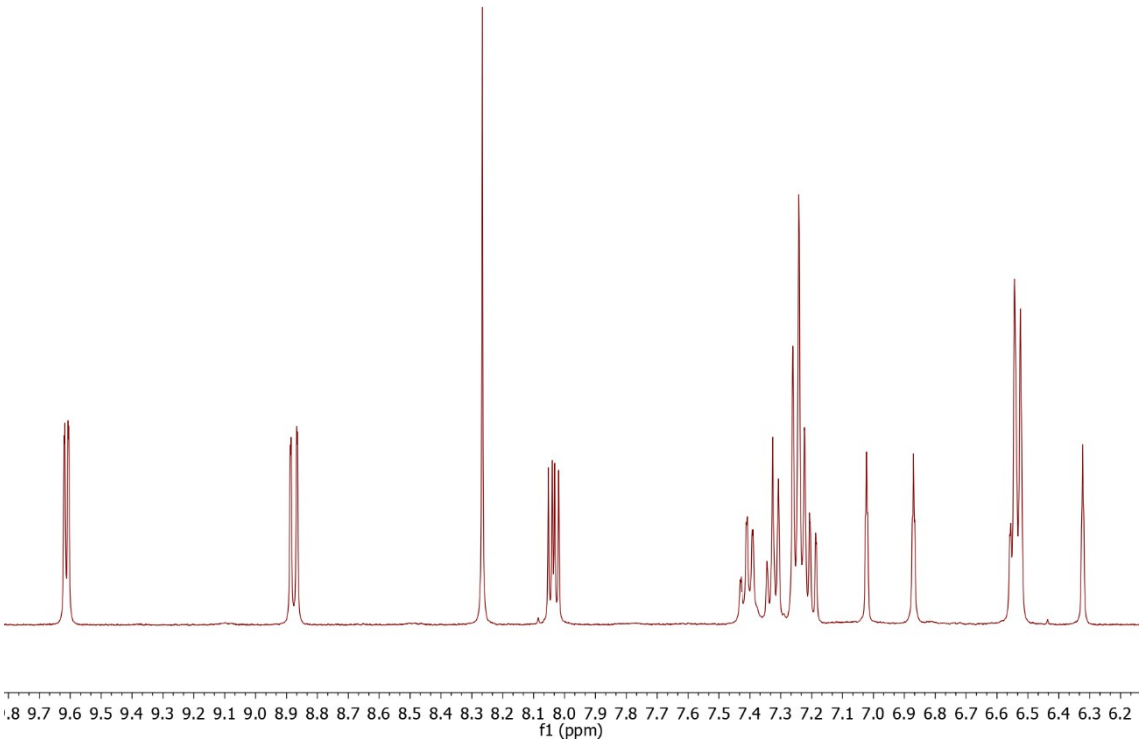

Fig. S12. ^{1}H-NMR spectrum of *fac*-[Mn(CO)$_3$(CTZ)(phen)](PF$_6$), DMSO-d$_6$ solution.

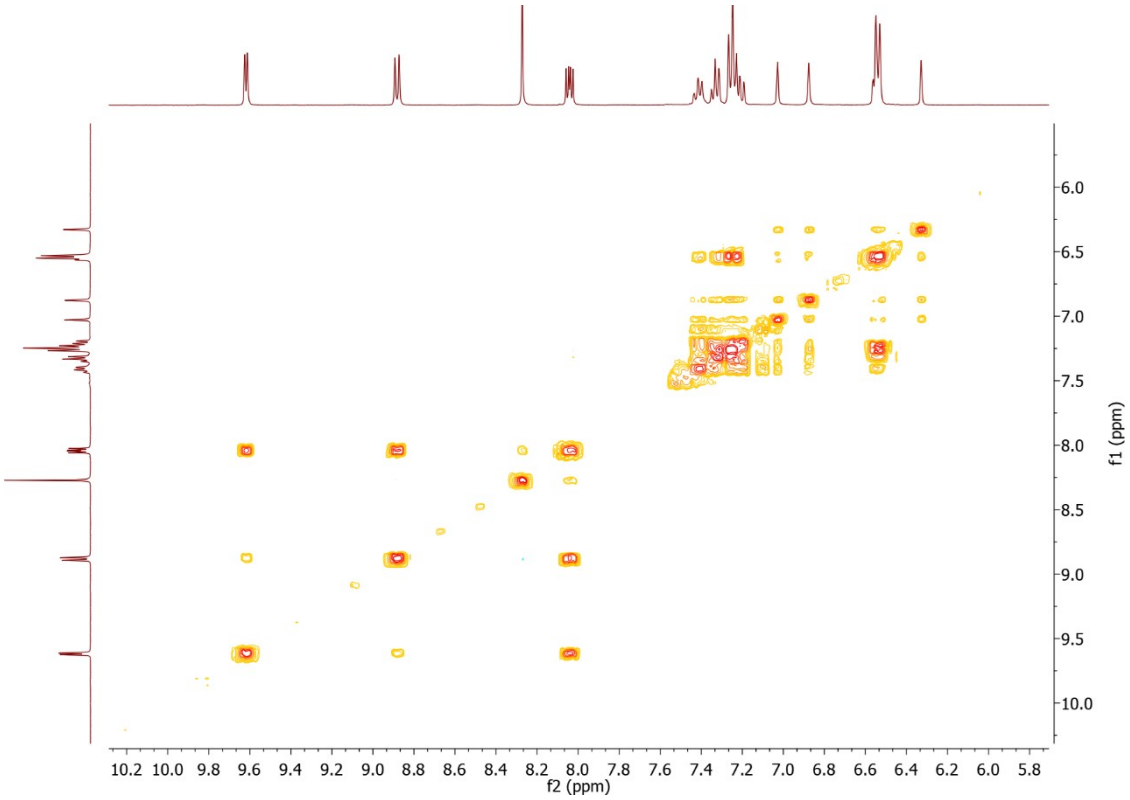

Fig. S13. ^{1}H-^{1}H-NMR (COSY) spectrum of *fac*-[Mn(CO)$_3$(CTZ)(phen)](PF$_6$), DMSO-d$_6$ solution.

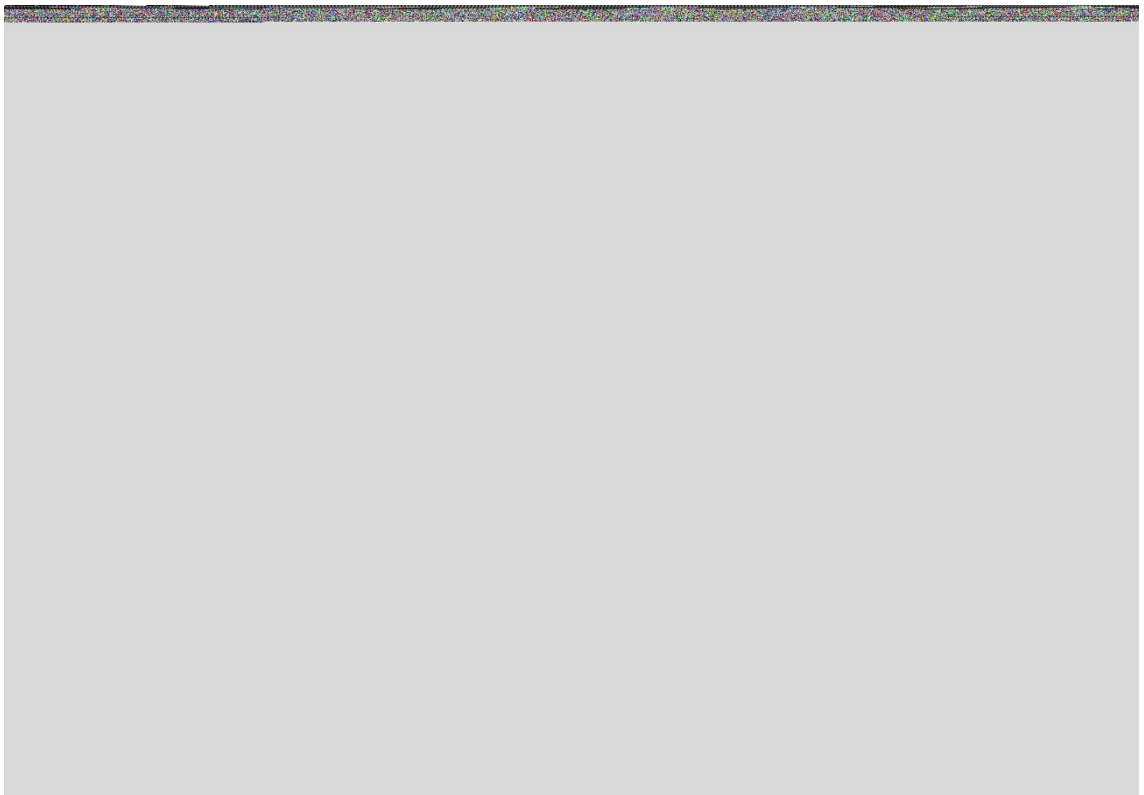

Fig. S14. ^{31}P-NMR spectrum of *fac*-[MnBr(CO)$_3$(CTZ)(phen)](PF$_6$), DMSO-d$_6$ solution.

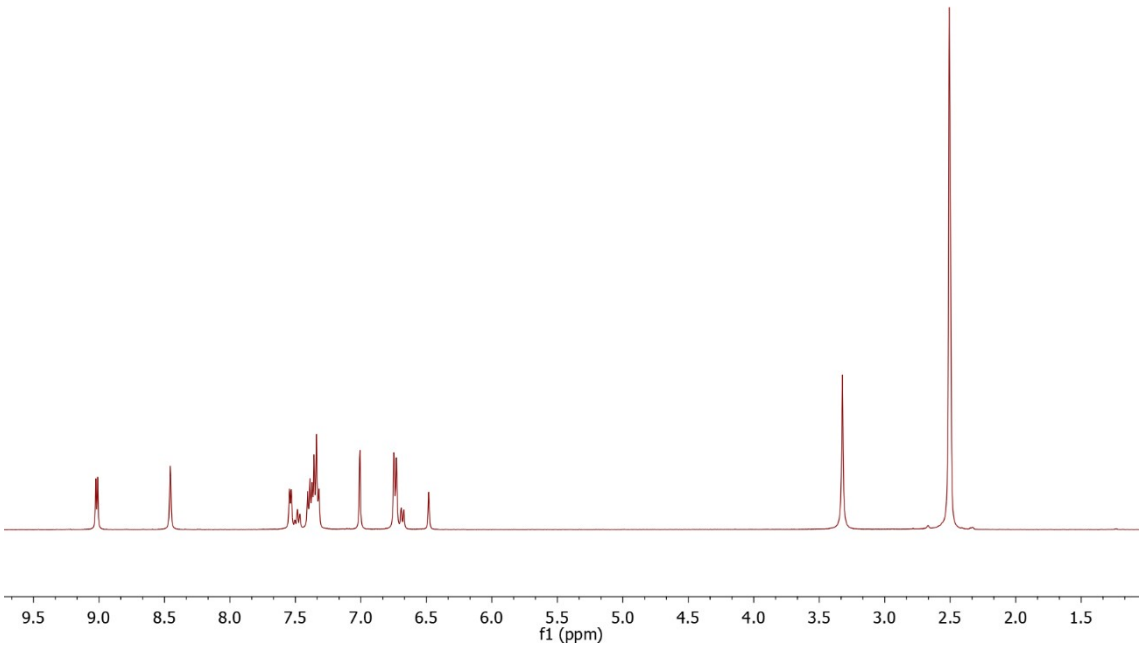

Fig. S15. ^{1}H-NMR spectrum of *fac*-[Mn(CO)$_3$(CTZ)(dmb)](PF$_6$), DMSO-d$_6$ solution.

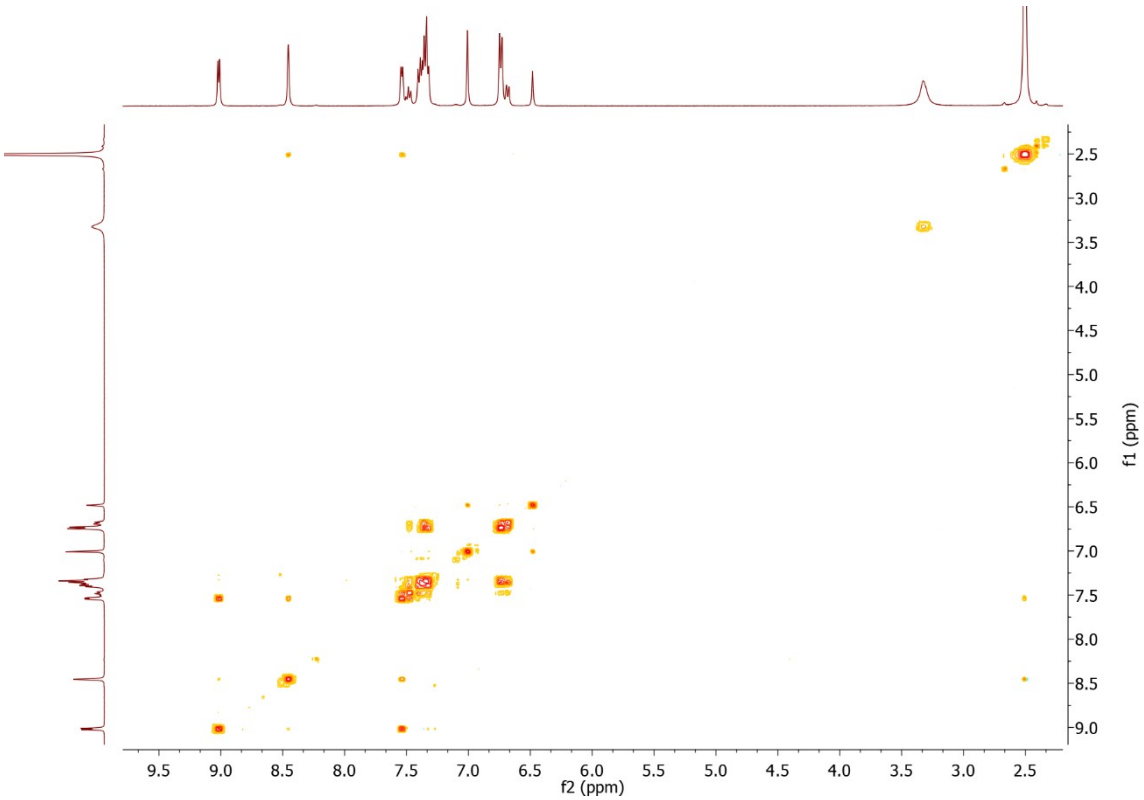

Fig. S16. ^{1}H-^{1}H-NMR (COSY) spectrum of *fac*-[Mn(CO)$_3$(CTZ)(dmb)](PF$_6$), DMSO-d$_6$ solution.

Fig. S17. ^{31}P-NMR spectrum of *fac*-[Mn(CO)$_3$(CTZ)(dmb)](PF$_6$), DMSO-d$_6$ solution.

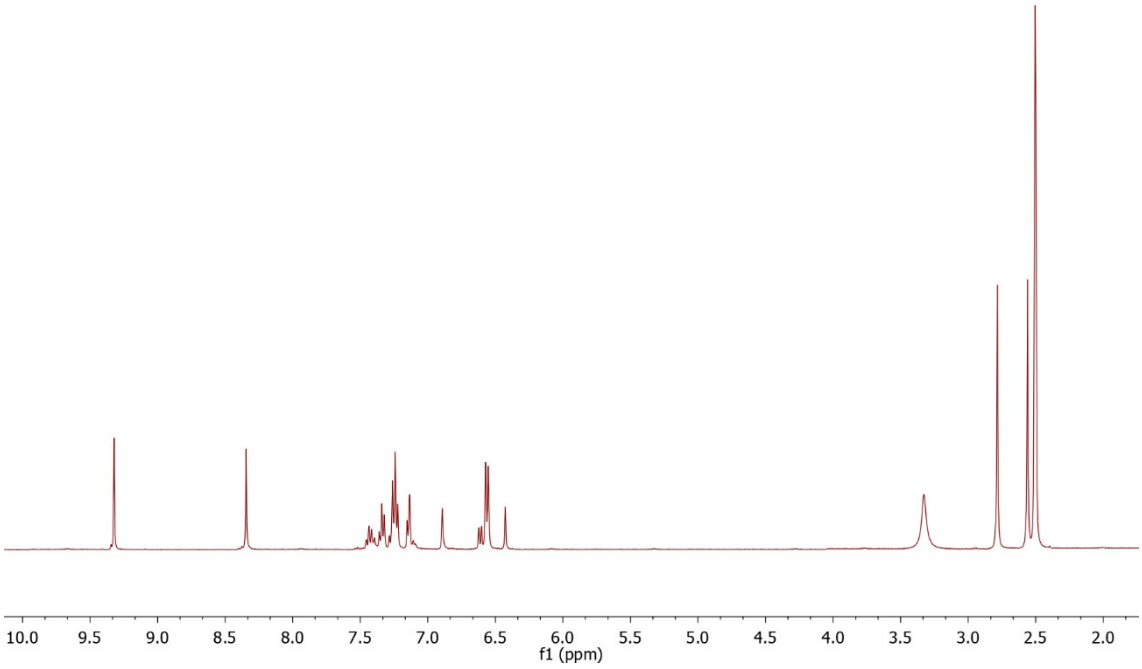

Fig. S18. ^{1}H-NMR spectrum of *fac*-[Mn(CO)$_3$(CTZ)(tmp)](PF$_6$), DMSO-d$_6$ solution.

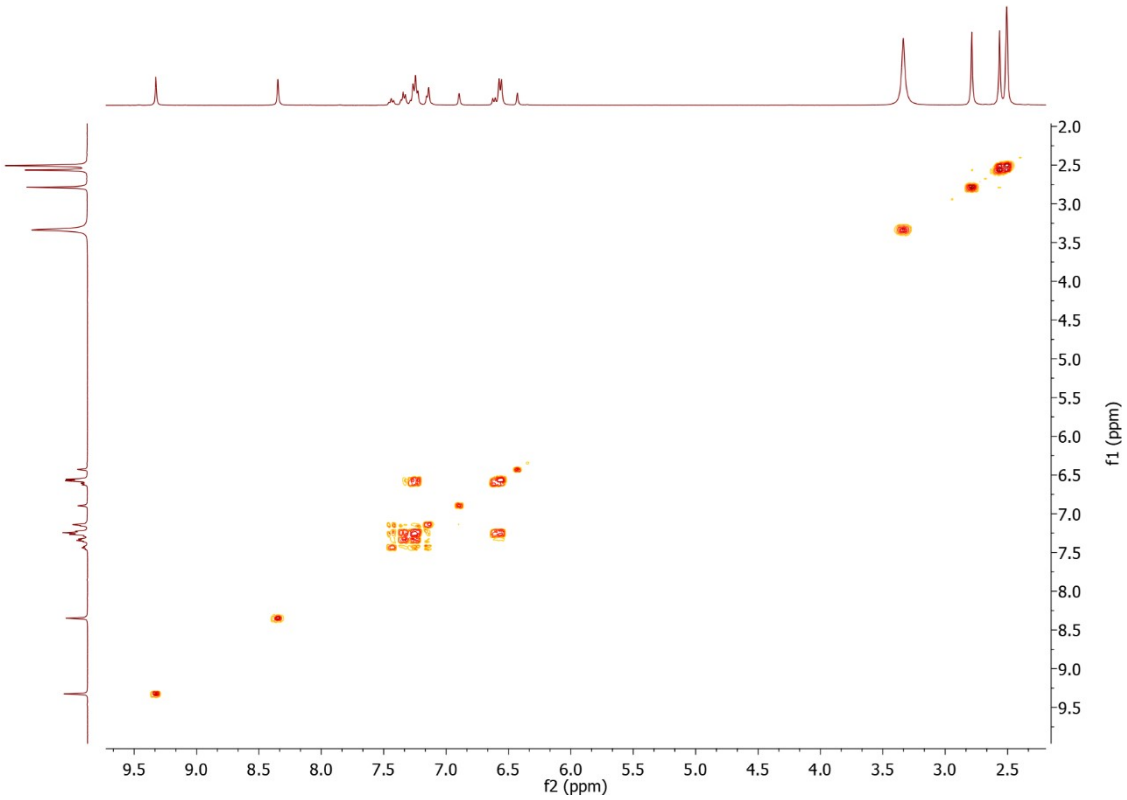

Fig. S19. ^{1}H-^{1}H-NMR (COSY) spectrum of *fac*-[Mn(CO)$_3$(CTZ)(tmp)](PF$_6$), DMSO-d$_6$ solution.

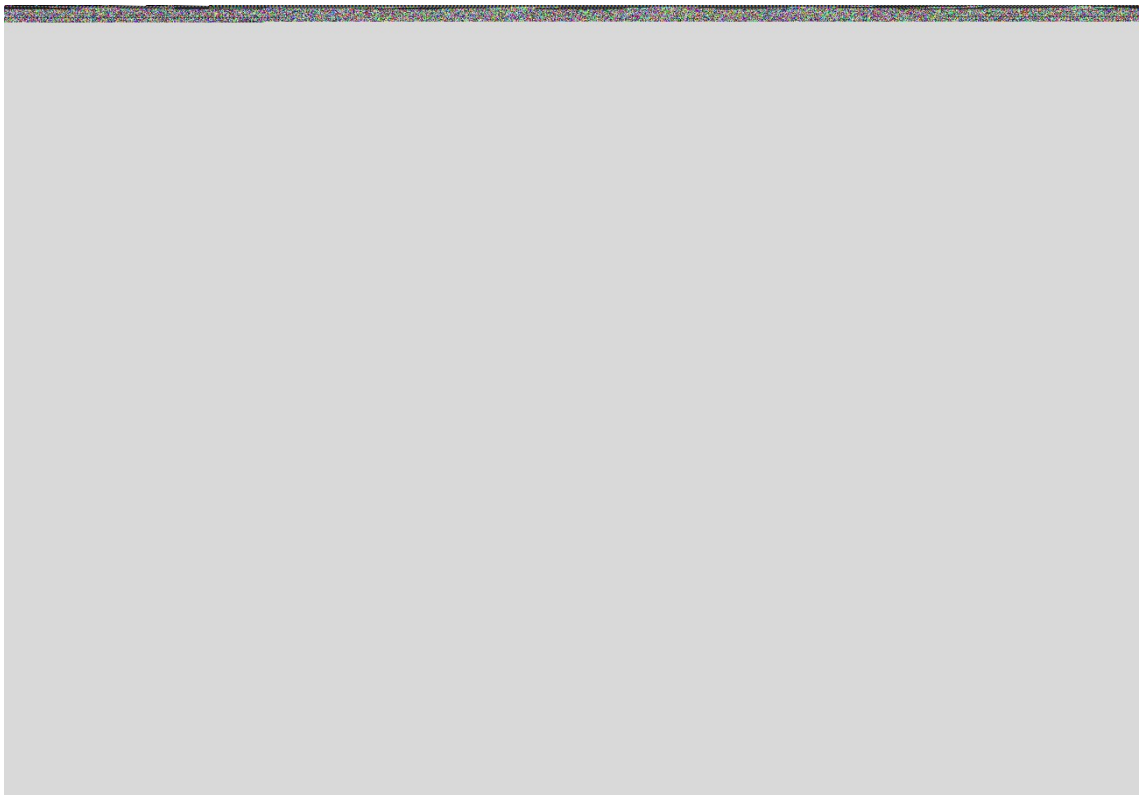

Fig. S20. ^{31}P-NMR spectrum of *fac*-[Mn(CO)$_3$(CTZ)(tmp)](PF$_6$), DMSO-d$_6$ solution.

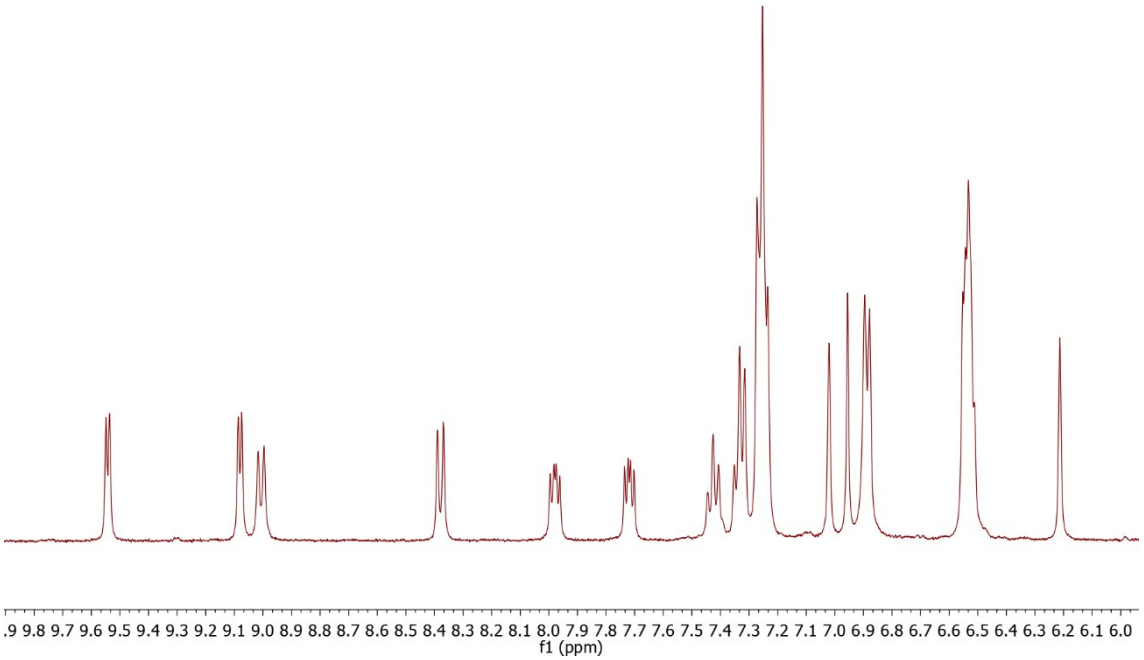

Fig. S21. ^{1}H-NMR spectrum of *fac*-[Mn(CO)$_3$(CTZ)(aminophen)](PF$_6$), DMSO-d$_6$ solution.

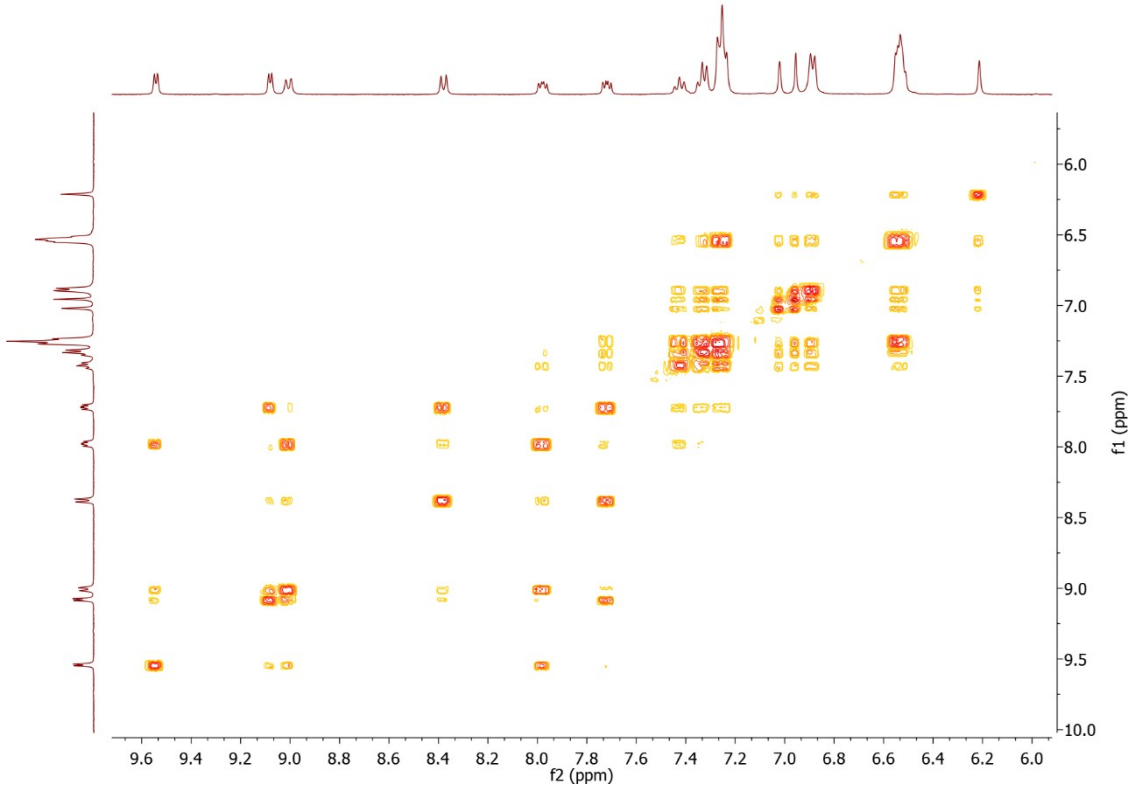

Fig. S22. ^{1}H-^{1}H-NMR (COSY) spectrum of *fac*-[Mn(CO)$_3$(CTZ)(aminophen)](PF$_6$), DMSO-d$_6$ solution.

Fig. S23. ^{31}P-NMR spectrum of *fac*-[Mn(CO)$_3$(CTZ)(aminophen)](PF$_6$), DMSO-d$_6$ solution.

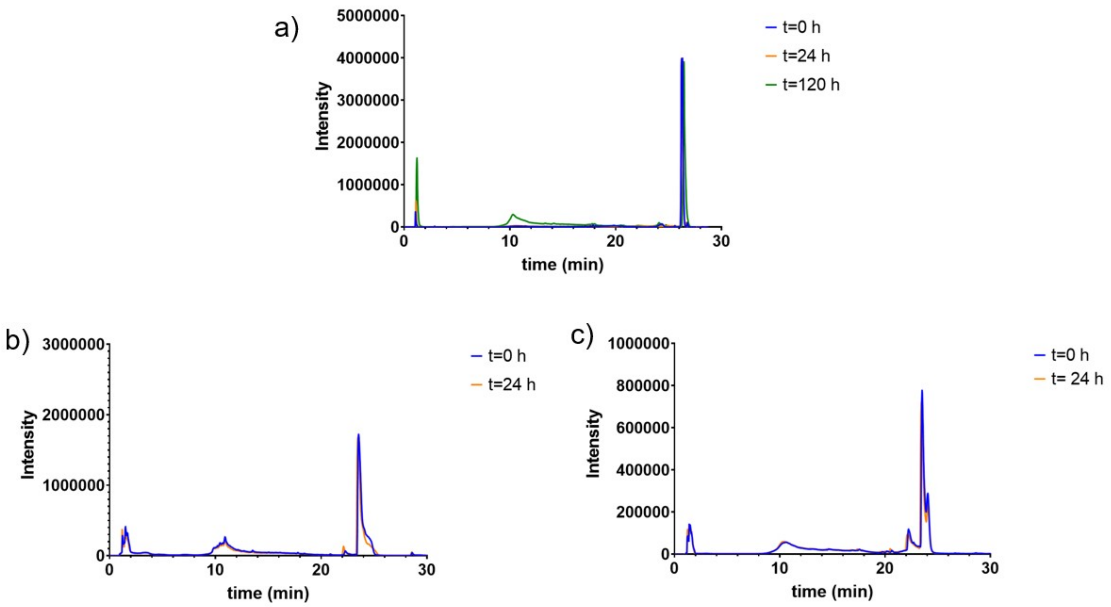

Fig. S24. Chromatograms obtained in the stability study at different times for *fac*-[Mn(CO)$_3$(CTZ)(tmp)](PF$_6$) in different media: a) DMSO, b) DMSO:BHI 50:50, c) DMSO:FBS 50:50.

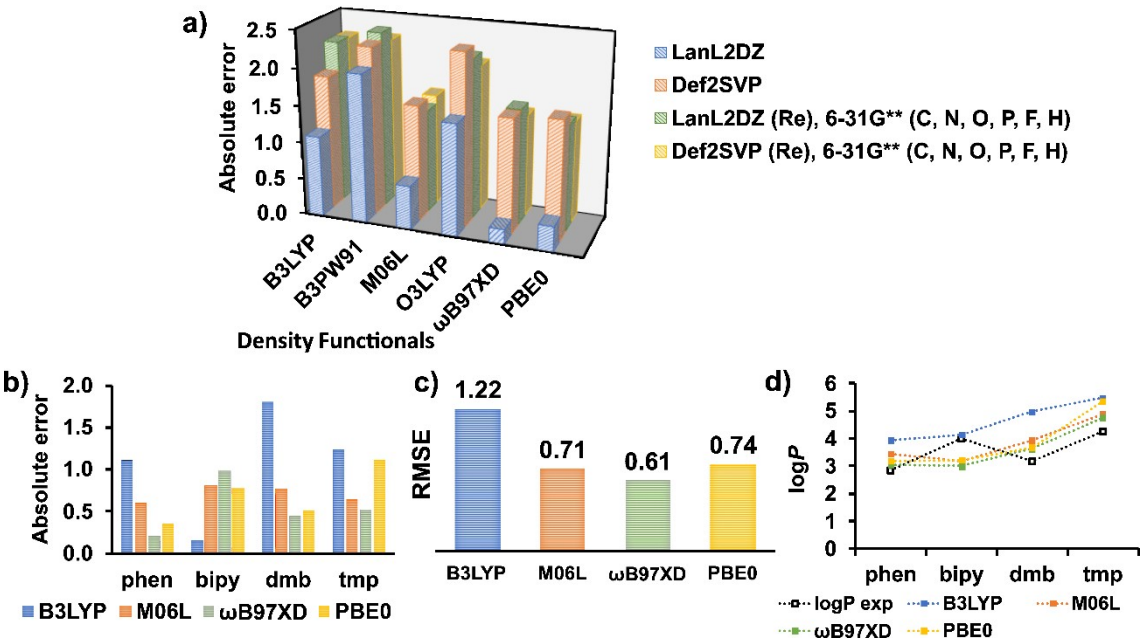

Fig. S25. a) Absolute errors of logP_{calc} for *fac*-[Re(CO)$_3$(CTZ)(phen)]$^+$. b) Absolute errors of logP_{calc} for *fac*-[Re(CO)$_3$(CTZ)(NN)](PF$_6$) (basis set = LANL2DZ). c) RMSE of logP_{calc} of *fac*-[Re(CO)$_3$(CTZ)(NN)](PF$_6$) calculated using different functionals (basis set = LANL2DZ). d) Trends in logP_{calc} and logP_{exp} values for the Re(I) complexes as the NN ligand changes (basis set = LANL2DZ). NN = phen, bipy, dmb and tmp. The SMD solvation model was applied throughout.

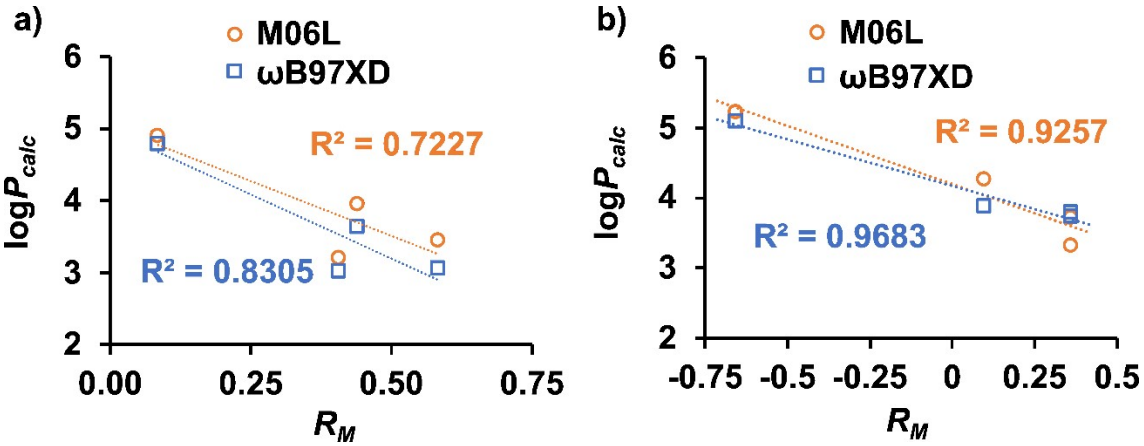

Fig. S26. logP_{calc} *vs.* R_M of Re(I) (a) and Mn(I) (b) tricarbonyl complexes. The logP_{calc} values were calculated using M06L/LANL2DZ and ωB97XD/LANL2DZ, respectively. Aminophen compounds were excluded from the analysis.

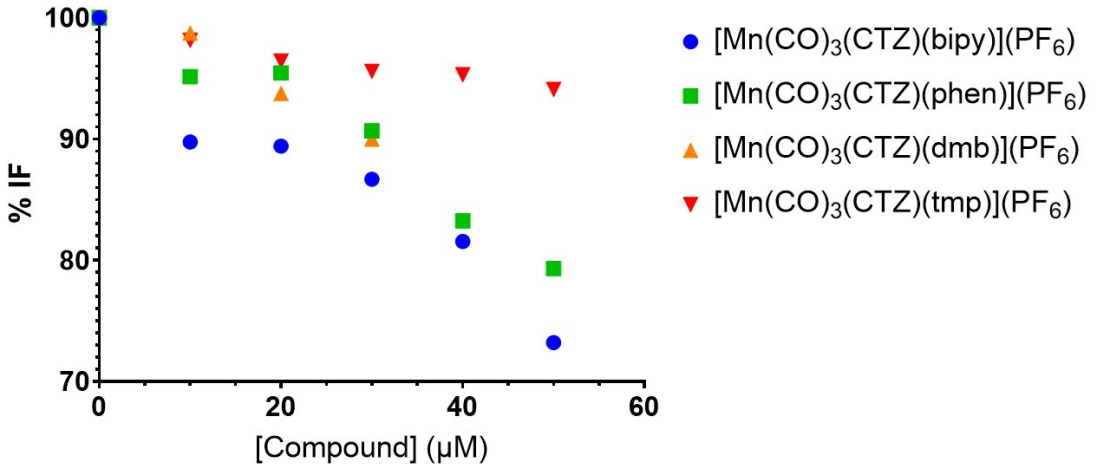

Fig. S27. Fluorescence quenching of the {DNA-EB} adduct by the Mn compounds. Relative fluorescence intensity (%) at the wavelength of maximum emission of the {DNA-EB} adduct.

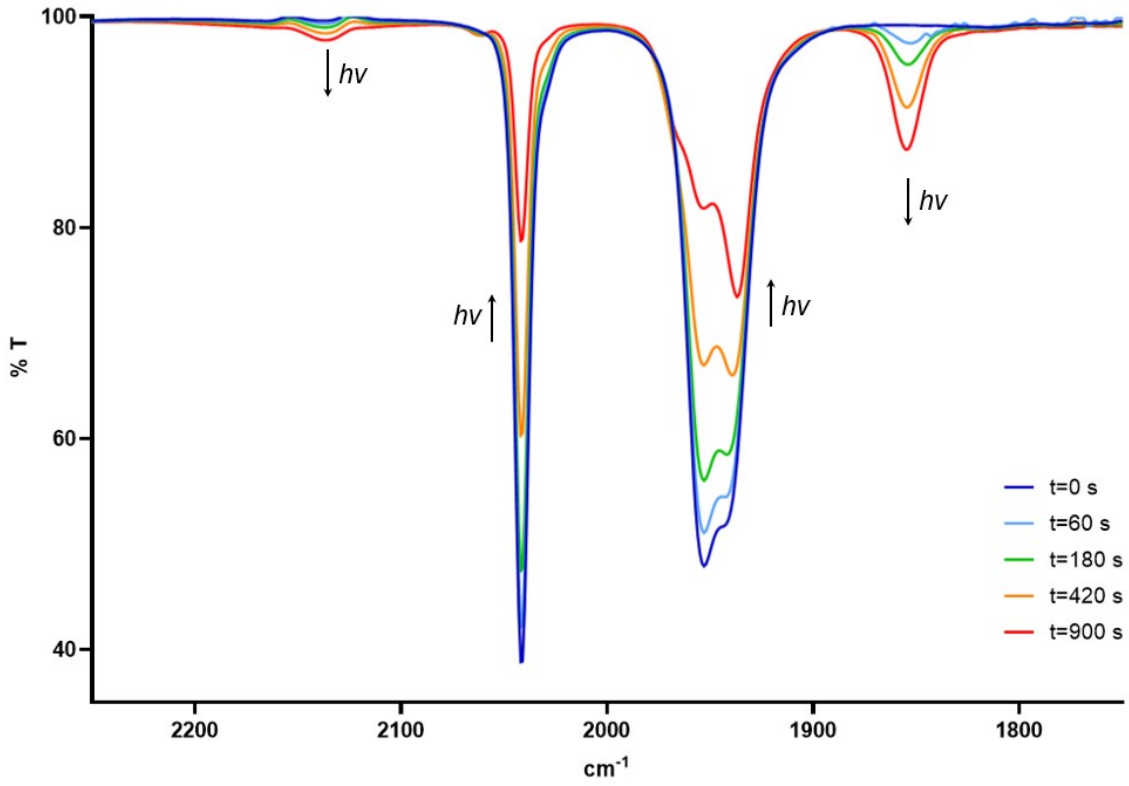

Fig. S28. FTIR spectra of *fac*-[Mn(CO)$_3$(CTZ)(phen)](PF$_6$) 1x10^{-3} M in CH_2Cl_2 solution after 0-900 s of irradiation at 395 ± 10 nm.

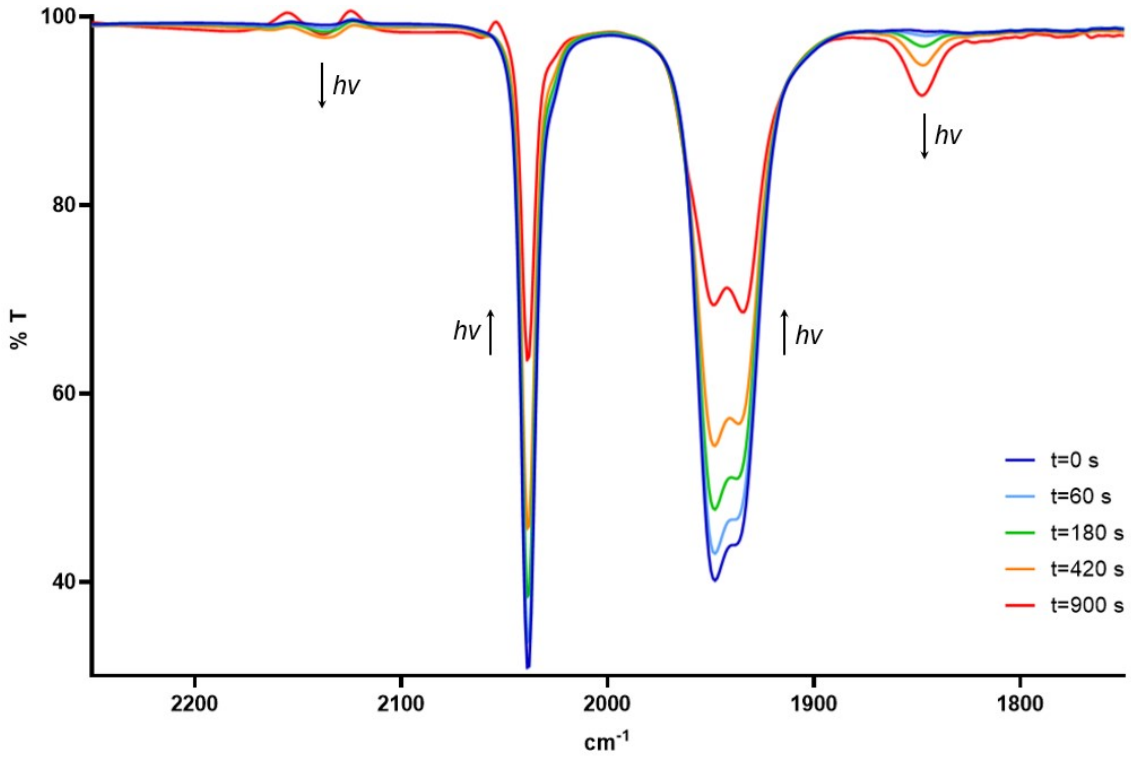

Fig. S29. FTIR spectra of *fac*-[$Mn(CO)_3(CTZ)(tmp)](PF_6)$ 1x10^{-3} M in CH_2Cl_2 solution after 0-900 s of irradiation at 395 ± 10 nm.

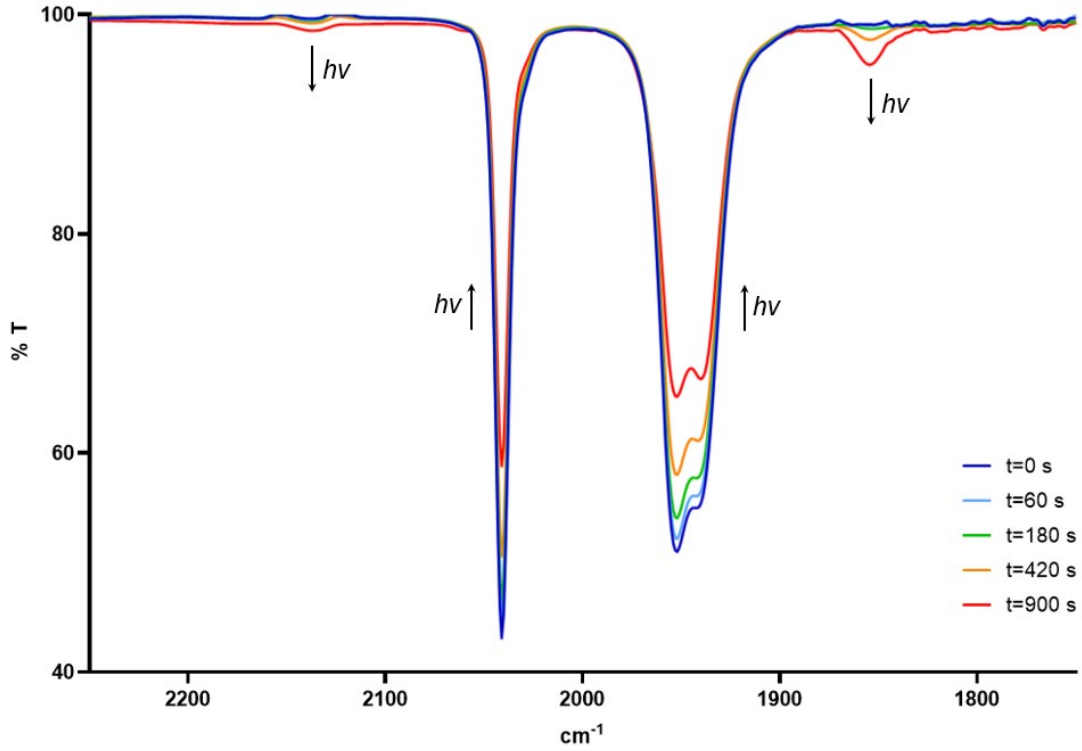

Fig. S30. FTIR spectra of *fac*-[$Mn(CO)_3(CTZ)(bipy)](PF_6)$ 1x10^{-3} M in CH_2Cl_2 solution after 0-900 s of irradiation at 395 ± 10 nm.

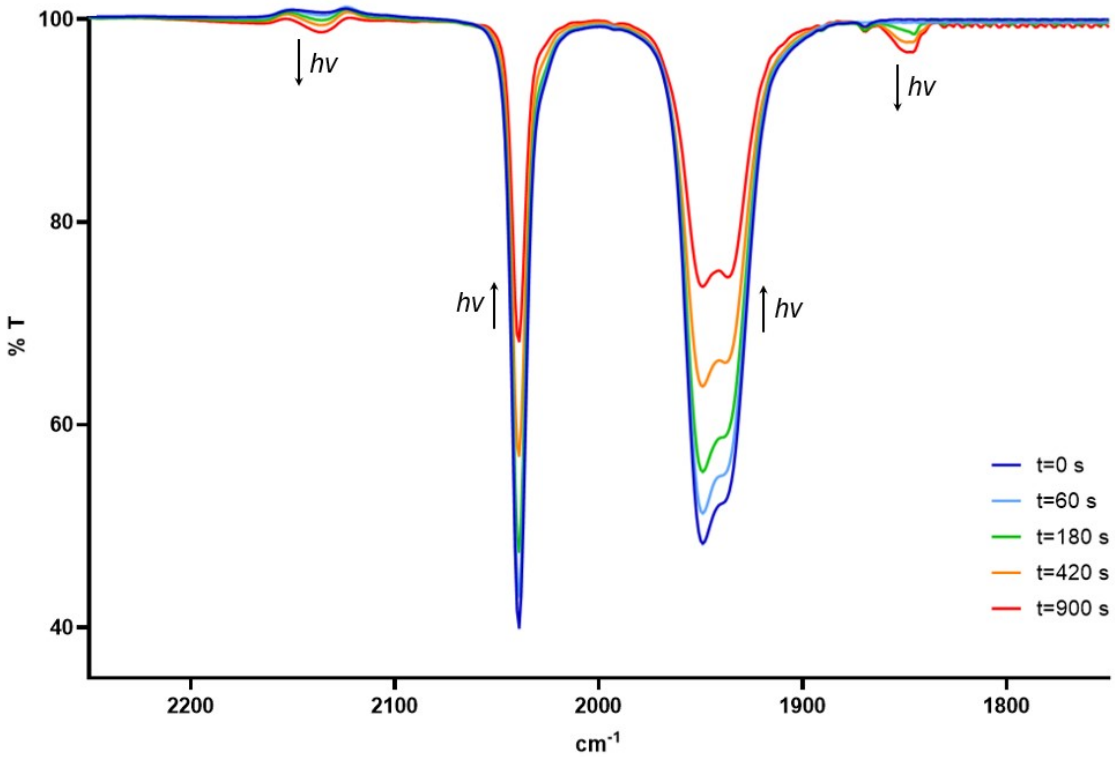

Fig. S31. FTIR spectra of *fac*-[$Mn(CO)_3(CTZ)(dmb)](PF_6)$ $1x10^{-3}$ M in CH_2Cl_2 solution after 0-900 s of irradiation at 395 ± 10 nm.

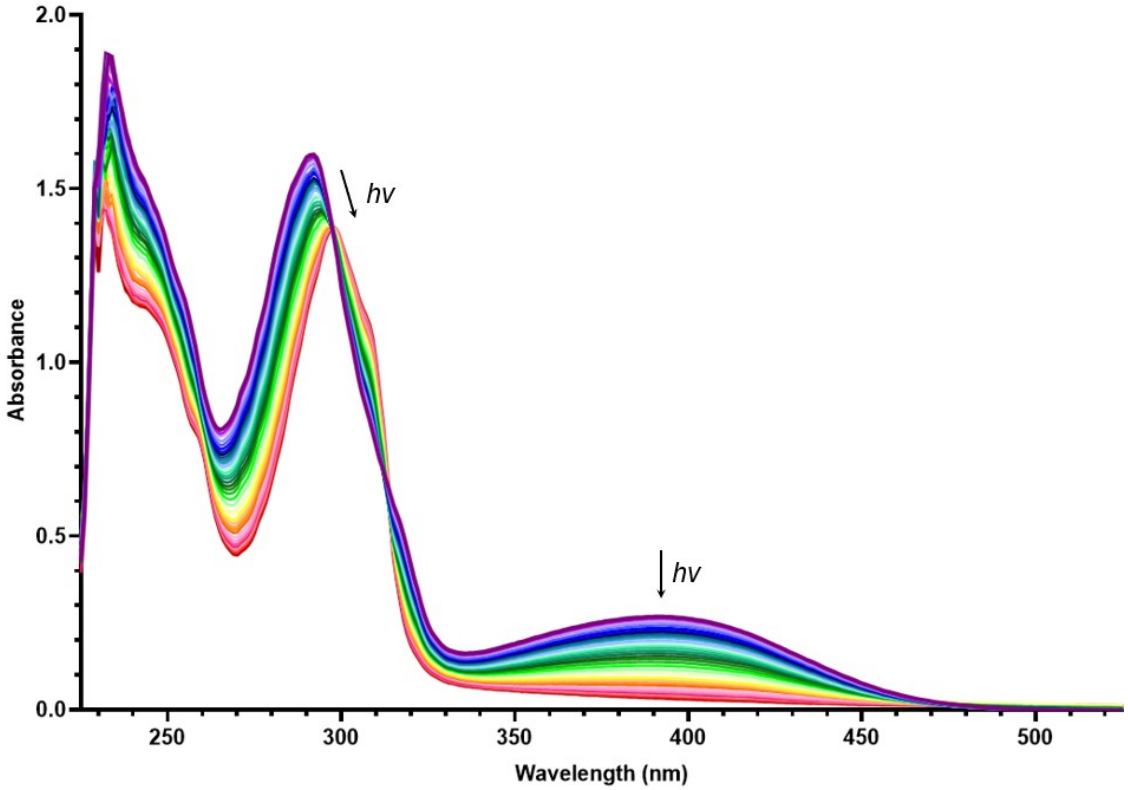

Fig. S32. UV-Vis spectra of *fac*-[$Mn(CO)_3(CTZ)(bipy)](PF_6)$ in CH_2Cl_2 solution after 0-3400 s of irradiation at 395 ± 10 nm.

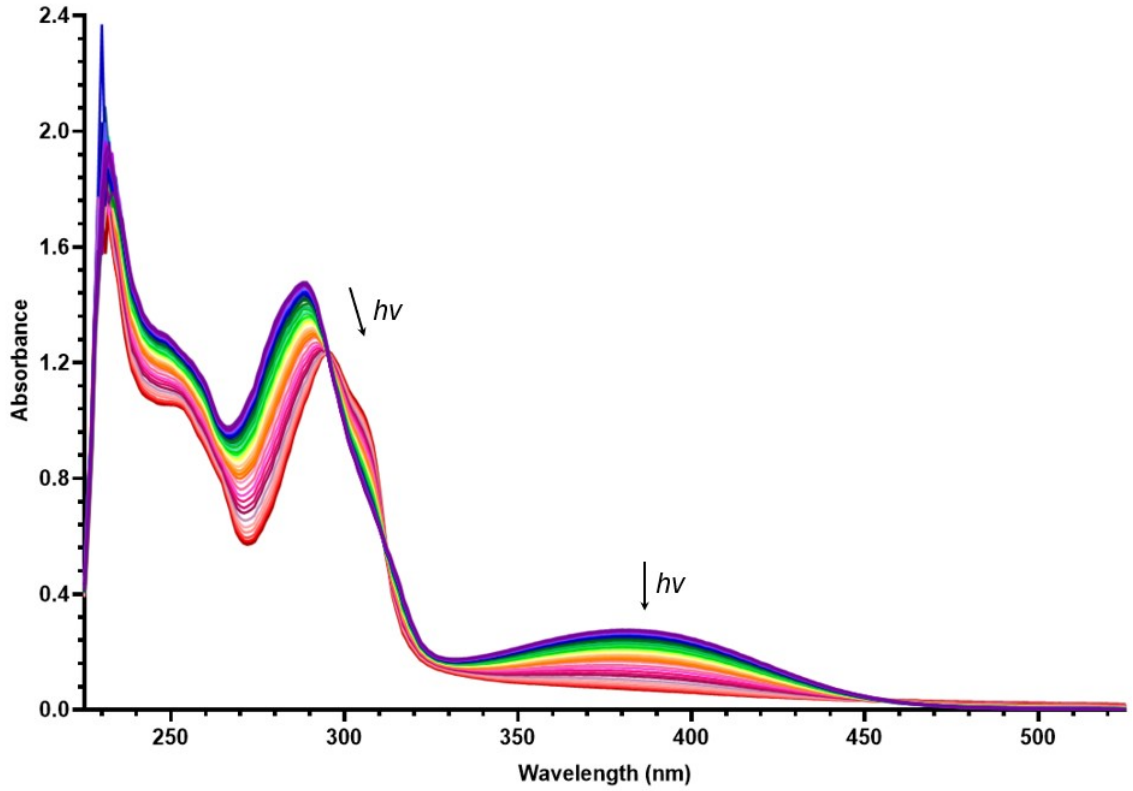

Fig. S33. UV-Vis spectra of *fac*-[$Mn(CO)_3(CTZ)(dmb)$](PF_6) in CH_2Cl_2 solution after 0-3700 s of irradiation at 395 ± 10 nm.

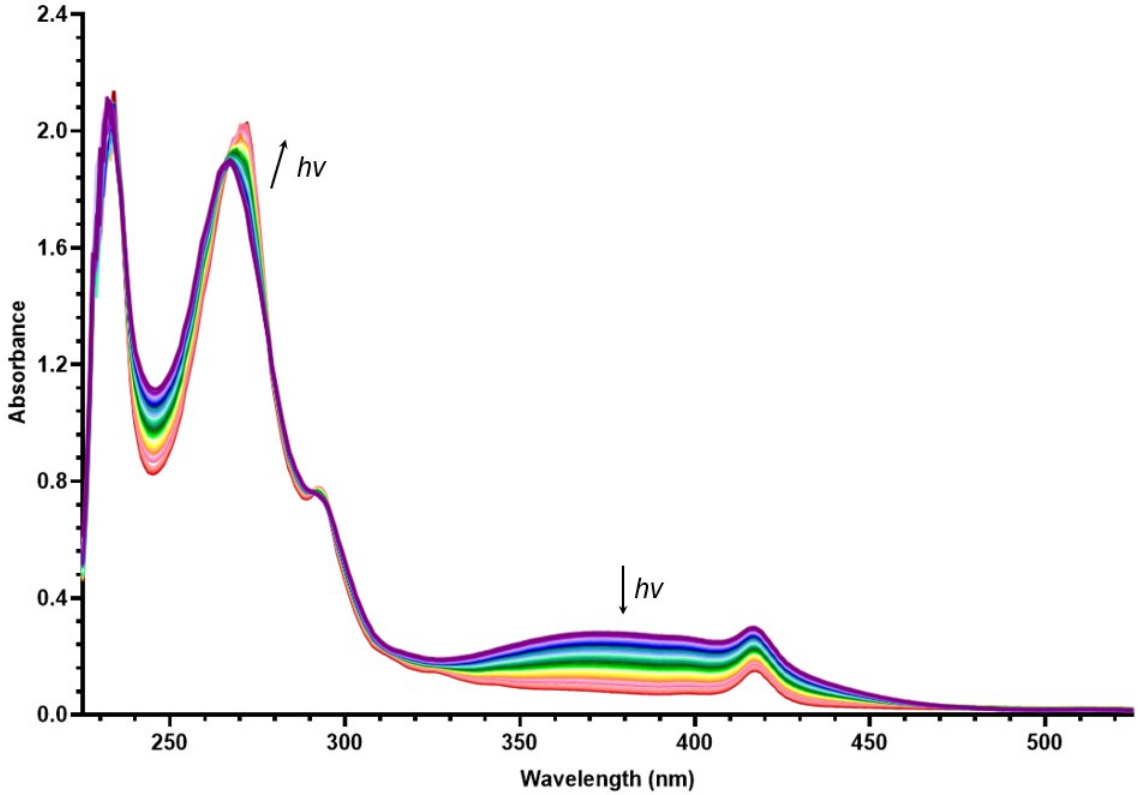

Fig. S34 UV-Vis spectra of *fac*-[$Mn(CO)_3(CTZ)(phen)$](PF_6) in CH_2Cl_2 solution after 0-4660 s of irradiation at 395 ± 10 nm.

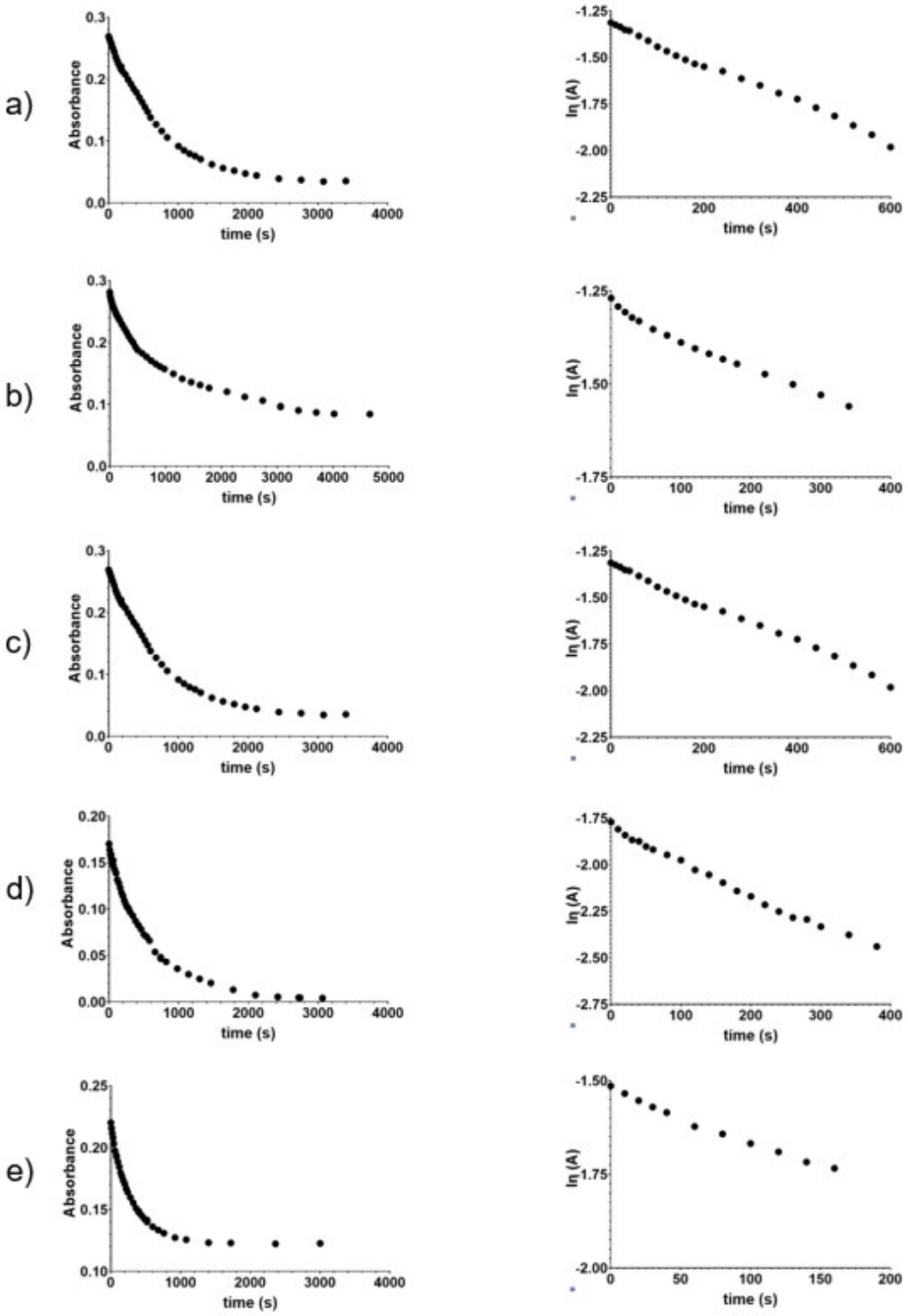

Fig. S35. Absorbance *vs* time of irradiation (left) and ln(Absorbance) *vs* time of irradiation (right) at 395 ± 10 nm for the compounds: a) *fac*-[$Mn(CO)_3(CTZ)(bipy)](PF_6)$, b) *fac*-[$Mn(CO)_3(CTZ)(phen)](PF_6)$, c) *fac*-[$Mn(CO)_3(CTZ)(dmb)](PF_6)$, d) *fac*-[$Mn(CO)_3(CTZ)(tmp)](PF_6)$, e) *fac*-[$Mn(CO)_3(CTZ)(aminophen)](PF_6)$.

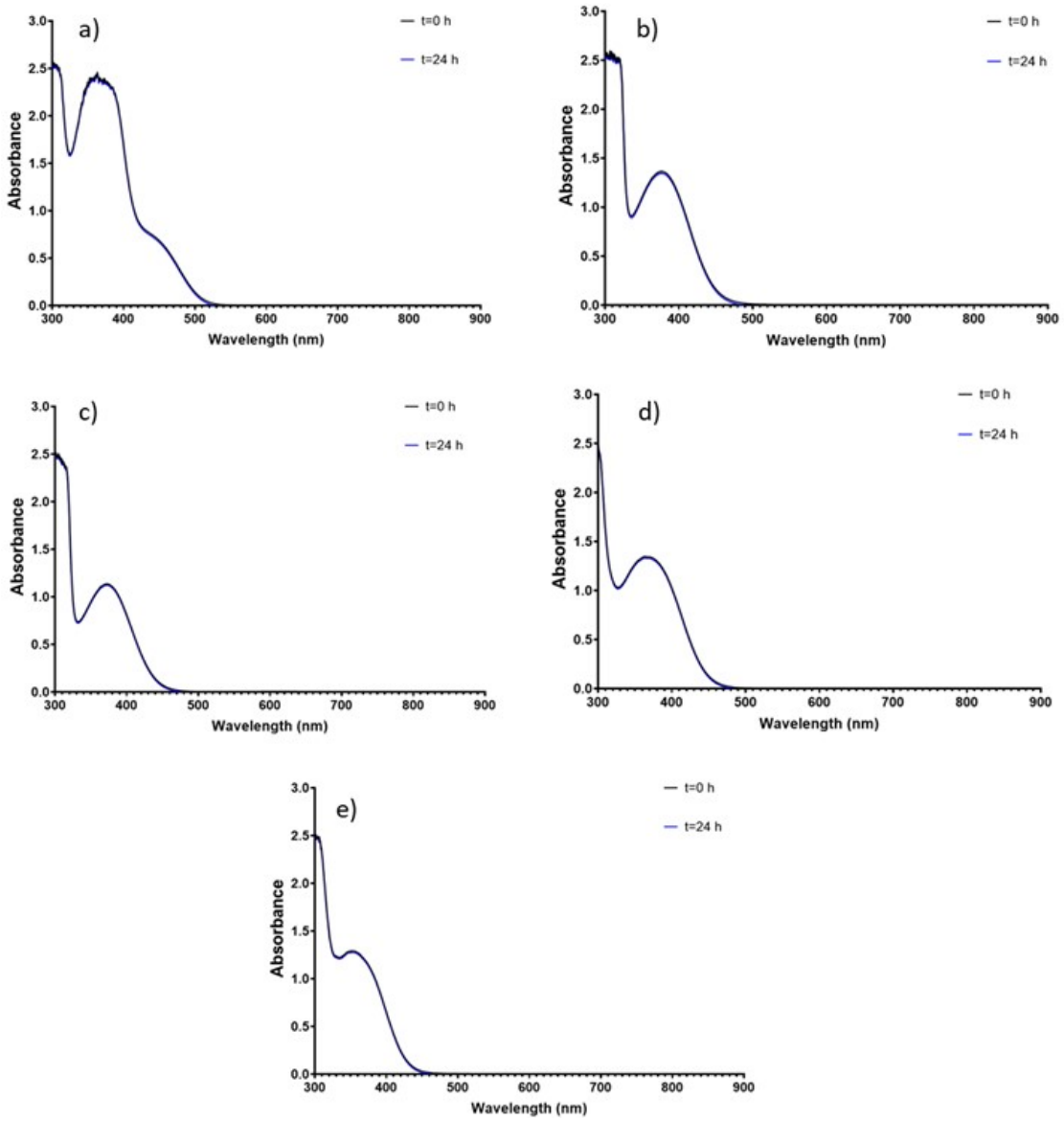

Fig. S36. UV-vis spectra of the Mn compounds at t=0 h (black) and t=24 h (blue) incubated in absence of light at 0.5 mM in DMSO:buffer phosphate 40 mM pH 7.4 (50:50). a) *fac*-[$Mn(CO)_3$(CTZ)(aminophen)](PF_6), **b)** *fac*-[$Mn(CO)_3$(CTZ)(bipy)](PF_6), **c)** *fac*-[$Mn(CO)_3$(CTZ)(dmb)](PF_6), **d)** *fac*-[$Mn(CO)_3$(CTZ)(phen)](PF_6), **e)** *fac*-[$Mn(CO)_3$(CTZ)(tmp)](PF_6).

Table S1. Gradient conditions for RP-HPLC-DAD for stability assessment

Time (min)	A (%)	B (%)
0-3	100	0
3-6	100-75	0-25
6-9	75-66	25-34
9-20	66-0	34-100
20-27	0	100
27-30	0-100	100-0

Table S2. Free energies (Hartree) and log*P* for *fac*-[Re(CO)$_3$(CTZ)(phen)]$^+$, calculated using B3LYP, B3PW91, M06L, O3LYP, ωB97XD or PBE0 functional, in conjunction with Def2SVP, LANL2DZ (Re)/6-31G** (C, N, O, P, F, H) or Def2SVP (Re)/6-31G** (C, N, O, P, F, H) basis set. In all cases, the SMD solvation model was used.

Basis set	Density functional	Compound	Sum of electronic and thermal Free Energies (Hartree)		log*P*
			Water	n-Octanol	
Def2SVP	B3LYP	PF_6^-	-940.193818	-940.190924	
		fac-[Re(CO)$_3$(CTZ)(phen)]$^+$	-2406.303775	-2406.316811	4.67
	B3PW91	PF_6^-	-939.930328	-939.927412	
		fac-[Re(CO)$_3$(CTZ)(phen)]$^+$	-2405.589605	-2405.603653	5.12
	M06L	PF_6^-	-940.116515	-940.113590	
		fac-[Re(CO)$_3$(CTZ)(phen)]$^+$	-2406.135898	-2406.148422	4.42
	O3LYP	PF_6^-	-939.972437	-939.969548	
		fac-[Re(CO)$_3$(CTZ)(phen)]$^+$	-2405.720713	-2405.734862	5.18
	ωB97XD	PF_6^-	-940.021221	-940.018295	
		fac-[Re(CO)$_3$(CTZ)(phen)]$^+$	-2405.718559	-2405.731051	4.40
	PBE0	PF_6^-	-939.501351	-939.498406	
		fac-[Re(CO)$_3$(CTZ)(phen)]$^+$	-2403.985887	-2403.998521	4.46
LANL2DZ (Re), 6-31G** (C, N, O, P, F, H)	B3LYP	PF_6^-	-940.736946	-940.733983	
		fac-[Re(CO)$_3$(CTZ)(phen)]$^+$	-2408.558319	-2408.572261	5.05
	B3PW91	PF_6^-	-940.473665	-940.470674	
		fac-[Re(CO)$_3$(CTZ)(phen)]$^+$	-2407.839033	-2407.853392	5.23
	M06L	PF_6^-	-940.668012	-940.665036	
		fac-[Re(CO)$_3$(CTZ)(phen)]$^+$	-2408.395479	-2408.407694	4.25
	O3LYP	PF_6^-	-940.514832	-940.511866	
		fac-[Re(CO)$_3$(CTZ)(phen)]$^+$	-2407.976170	-2407.990041	5.02
	ωB97XD	PF_6^-	-940.568437	-940.565439	
		fac-[Re(CO)$_3$(CTZ)(phen)]$^+$	-2407.948737	-2407.961325	4.41
	PBE0	PF_6^-	-940.047839	-940.044813	
		fac-[Re(CO)$_3$(CTZ)(phen)]$^+$	-2406.256117	-2406.268480	4.30
Def2SVP (Re), 6-31G** (C, N, O, P, F, H)	B3LYP	PF_6^-	-940.736946	-940.733983	
		fac-[Re(CO)$_3$(CTZ)(phen)]$^+$	-2407.781217	-2407.795135	5.04
	B3PW91	PF_6^-	-940.473665	-940.470674	
		fac-[Re(CO)$_3$(CTZ)(phen)]$^+$	-2407.063688	-2407.077686	5.06
	M06L	PF_6^-	-940.668012	-940.665036	
		fac-[Re(CO)$_3$(CTZ)(phen)]$^+$	-2407.641144	-2407.653602	4.36
	O3LYP	PF_6^-	-940.514832	-940.511866	
		fac-[Re(CO)$_3$(CTZ)(phen)]$^+$	-2407.199233	-2407.212725	4.84
	ωB97XD	PF_6^-	-940.568437	-940.565439	
		fac-[Re(CO)$_3$(CTZ)(phen)]$^+$	-2407.200486	-2407.212696	4.24
	PBE0	PF_6^-	-940.047839	-940.044813	
		fac-[Re(CO)$_3$(CTZ)(phen)]$^+$	-2407.200486	-2407.212696	4.22

Table S3. Free energies (Hartree) and log*P* for *fac*-[Re(CO)$_3$(CTZ)(phen)]$^+$, *fac*-[Re(CO)$_3$(CTZ)(bipy)]$^+$, *fac*-[Re(CO)$_3$(CTZ)(dmb)]$^+$, *fac*-[Re(CO)$_3$(CTZ)(tmp)]$^+$ and *fac*-[Re(CO)$_3$(CTZ)(aminophen)]$^+$, calculated using B3LYP, B3PW91, M06L, O3LYP, ωB97XD or PBE0 functional and the LANL2DZ basis set. In all cases, the SMD solvation model was used.

Density functional	Compound	Sum of electronic and thermal Free Energies (Hartree)		log*P*
		Water	n-Octanol	
B3LYP	PF_6^-	-605.867035	-605.864544	-
	fac-[Re(CO)$_3$(CTZ)(phen)]$^+$	-1963.003523	-1963.014597	3.95
	fac-[Re(CO)$_3$(CTZ)(bipy)]$^+$	-1886.794591	-1886.806104	4.15
	fac-[Re(CO)$_3$(CTZ)(dmb)]$^+$	-1965.374217	-1965.387540	4.98
	fac-[Re(CO)$_3$(CTZ)(tmp)]$^+$	-2120.148686	-2120.163107	5.49
	fac-[Re(CO)$_3$(CTZ)(aminophen)]$^+$	-2018.347853	-2018.357297	3.20
B3PW91	PF_6^-	-605.659737	-605.657260	-
	fac-[Re(CO)$_3$(CTZ)(phen)]$^+$	-1962.358669	-1962.371702	4.86
M06L	PF_6^-	-605.774145	-605.771659	-
	fac-[Re(CO)$_3$(CTZ)(phen)]$^+$	-1962.835655	-1962.845629	3.44
	fac-[Re(CO)$_3$(CTZ)(bipy)]$^+$	-1886.632211	-1886.641639	3.19
	fac-[Re(CO)$_3$(CTZ)(dmb)]$^+$	-1965.198992	-1965.210053	3.94
	fac-[Re(CO)$_3$(CTZ)(tmp)]$^+$	-2119.962227	-2119.975367	4.90
	fac-[Re(CO)$_3$(CTZ)(aminophen)]$^+$	-2018.176280	-2018.184347	2.57
O3LYP	PF_6^-	-605.677097	-605.674634	-
	fac-[Re(CO)$_3$(CTZ)(phen)]$^+$	-1962.462137	-1962.474075	4.36
ωB97XD	PF_6^-	-605.705348	-605.702839	
	fac-[Re(CO)$_3$(CTZ)(phen)]$^+$	-1962.410220	-1962.419363	3.05
	fac-[Re(CO)$_3$(CTZ)(bipy)]$^+$	-1886.225508	-1886.234568	3.01
	fac-[Re(CO)$_3$(CTZ)(dmb)]$^+$	-1964.784703	-1964.795101	3.63
	fac-[Re(CO)$_3$(CTZ)(tmp)]$^+$	-2119.518459	-2119.531357	4.78
	fac-[Re(CO)$_3$(CTZ)(aminophen)]$^+$	-2017.739138	-2017.745221	1.64
PBE0	PF_6^-	-605.305218	-605.302720	-
	fac-[Re(CO)$_3$(CTZ)(phen)]$^+$	-1960.840850	-1960.850289	3.19
	fac-[Re(CO)$_3$(CTZ)(bipy)]$^+$	-1884.715324	-1884.724817	3.22
	fac-[Re(CO)$_3$(CTZ)(dmb)]$^+$	-1963.198150	-1963.208667	3.69
	fac-[Re(CO)$_3$(CTZ)(tmp)]$^+$	-2117.794888	-2117.809058	5.37
	fac-[Re(CO)$_3$(CTZ)(aminophen)]$^+$	-2016.127055	-2016.134864	2.44

Table S4. Free energies (Hartree) and log*P* for *fac*-[$Mn(CO)_3$(CTZ)(phen)]$^+$, *fac*-[$Mn(CO)_3$(CTZ)(bipy)]$^+$, *fac*-[$Mn(CO)_3$(CTZ)(dmb)]$^+$, *fac*-[$Mn(CO)_3$(CTZ)(tmp)]$^+$ and *fac*-[$Mn(CO)_3$(CTZ)(aminophen)]$^+$, calculated using M06L or ωB97XD functional and the LANL2DZ basis set. In all cases the SMD solvation model was used.

Density functional	Compound	Sum of electronic and thermal Free Energies (Hartree)		log*P*
		Water	n-Octanol	
ωB97XD	PF_6^-	-605.705348	-605.702839	
	fac-[$Mn(CO)_3$(CTZ)(phen)]$^+$	-1987.137043	-1987.147776	3.78
	fac-[$Mn(CO)_3$(CTZ)(bipy)]$^+$	-1910.953999	-1910.964620	3.73
	fac-[$Mn(CO)_3$(CTZ)(dmb)]$^+$	-1989.512130	-1989.523063	3.88
	fac-[$Mn(CO)_3$(CTZ)(tmp)]$^+$	-2144.243830	-2144.257384	5.08
	fac-[$Mn(CO)_3$(CTZ)(aminophen)]$^+$	-2042.467558	-2042.474430	2.01
M06L	PF_6^-	-605.774145	-605.771659	
	fac-[$Mn(CO)_3$(CTZ)(phen)]$^+$	-1987.637684	-1987.648248	3.72
	fac-[$Mn(CO)_3$(CTZ)(bipy)]$^+$	-1911.437090	-1911.446776	3.31
	fac-[$Mn(CO)_3$(CTZ)(dmb)]$^+$	-1990.002681	-1990.014439	4.27
	fac-[$Mn(CO)_3$(CTZ)(tmp)]$^+$	-2144.765337	-2144.779176	5.22
	fac-[$Mn(CO)_3$(CTZ)(aminophen)]$^+$	-2042.978989	-2042.987742	2.88

Table S5. Free energies (Hartree) and log*P* for *fac*-[Re(CO)$_3$(CTZ)(aminophen)]$^+$ and *fac*-[Mn(CO)$_3$(CTZ)(aminophen)]$^+$, calculated using M06L or ωB97XD functional and the LANL2DZ basis set. In all cases the SMD solvation model was used with the addition of two explicit water molecules.

Density functional	Compound	Sum of electronic and thermal Free Energies (Hartree)		log*P*
		Water	n-Octanol	
M06L	PF_6^-	-605.774145	-605.771659	-
	fac-[Re(CO)$_3$(CTZ)(aminophen)]$^+$ + 2 H_2O	-2170.988169	-	4.53
	fac-[Re(CO)$_3$(CTZ)(aminophen)]$^+$ + 2 n-Octanol	-	-2799.350767	
	2 H_2O	-152.820982	-	
	2 n-Octanol	-	-781.171250	
	fac-[Mn(CO)$_3$(CTZ)(aminophen)]$^+$ + 2 H_2O	-2195.791363	-	4.37
	fac-[Mn(CO)$_3$(CTZ)(aminophen)]$^+$ + 2 n-Octanol	-	-2824.150231	
	2 H_2O	-152.820945	-	
	2 n-Octanol	-	-781.167838	
ωB97XD	PF_6^-	-605.705348	-605.702839	-
	fac-[Re(CO)$_3$(CTZ)(aminophen)]$^+$ + 2 H_2O	-2170.534559	-	7.41
	fac-[Re(CO)$_3$(CTZ)(aminophen)]$^+$ + 2 n-Octanol	-	-2798.835637	
	2 H_2O	-152.803621	-	
	2 n-Octanol	-	-781.086072	
	fac-[Mn(CO)$_3$(CTZ)(aminophen)]$^+$ + 2 H_2O	-2195.260587	-	6.98
	fac-[Mn(CO)$_3$(CTZ)(aminophen)]$^+$ + 2 n-Octanol	-	-2823.562112	
	2 H_2O	-152.802154	-	
	2 n-Octanol	-	-781.086000	

Table S6. R_M and calculated log*P* values (M06L-SMD/LANL2DZ and ωB97XD-SMD/LANL2DZ) for the Mn(I) and Re(I) analogues.

	Mn(I)			Re(I)			
NN	M06L	ωB97XD	R_M	M06L	ωB97XD	logP_{exp}	R_M
phen	3.72	3.78	0.364	3.44	3.05	2.85	0.585
bipy	3.31	3.73	0.363	3.19	3.01	4.00	0.409
dmb	4.27	3.88	0.099	3.94	3.63	3.18	0.442
tmp	5.22	5.08	-0.654	4.90	4.78	4.26	0.086
aminophen	4.37	6.98	0.169	4.53	7.41	-	0.178

Table S7. Nonpolar Surface area, DDEC6 dipole moment (ωB97XD-SMD/LANL2DZ) and experimental R_M of Re(I) tricarbonyl complexes.

NN	phen	bipy	dmb	tmp	aminophen
Nonpolar surface area (|ESP| <= 10 kcal/mol) (Å^2)	10.23	9.35	13.97	16.26	17.08
Nonpolar surface area (|ESP| <= 10 kcal/mol) (%)	1.89	1.76	2.47	2.72	3.08
Dipole moment (Debye)	14.48	14.41	15.53	15.18	16.61
R_M	0.585	0.409	0.442	0.086	0.178

Table S8. See attached file

Table S9. GO term enrichment analysis for downregulated proteins in *fac*-$[Mn(CO)_3(CTZ)(tmp)(PF_6)$ treated parasites. No enrichment was observed for upregulated proteins.

Biological Process				
ID	Name	Fold enrichment	*P*-value	Bonferroni
GO:0036211	protein modification process	2.58	0.007	0.086
GO:0140053	mitochondrial gene expression	50.61	0.019	0.236
GO:0002181	cytoplasmic translation	25.31	0.039	0.467
Molecular Function				
ID	Name	Fold enrichment	P-value	Bonferroni
GO:0003723	RNA binding	3.63	0.001	0.012
GO:0008135	translation factor activity, RNA binding	4.98	0.022	0.373
GO:0008289	lipid binding	7.79	0.027	0.455

Table S10. GO term enrichment analysis for downregulated proteins in *fac*-[$Re(CO)_3(CTZ)(tmp)](PF_6)$ treated parasites.

Biological Process				
ID	Name	Fold enrichment	*P*-value	Bonferroni
GO:0006520	cellular amino acid metabolic process	4.86	1,16E-11	2,21E-10
GO:0055086	nucleobase-containing small molecule metabolic process	3.96	7,33E-11	9,28E-10
GO:0005975	carbohydrate metabolic process	3.53	1,32E-07	1,00E-07
GO:0006575	cellular modified amino acid metabolic process	7.29	4,74E-05	3,00E-04
GO:0006399	tRNA metabolic process	2.9	7,47E-05	4,06E-04
GO:0006091	generation of precursor metabolites and energy	3.26	3,38E-04	1,61E-03
GO:0006766	vitamin metabolic process	12.16	5,54E-04	2,34E-03
GO:0006790	sulfur compound metabolic process	3.35	1,80E-03	6,85E-03
GO:0006457	protein folding	2.86	5,30E-03	1,83E-02
GO:0016071	mRNA metabolic process	2.78	6,38E-03	2,02E-02
GO:0006886	intracellular protein transport	1.94	2,41E-02	6,75E-02
GO:0007010	cytoskeleton organization	2.89	2,49E-02	6,75E-02
GO:0030163	protein catabolic process	1.96	2,85E-02	7,23E-02
GO:0002181	cytoplasmic translation	6.08	3,62E-02	8,61E-02
GO:0036211	protein modification process	1.31	4,94E-02	1,10E-01
Molecular Function				
GO:0043167	ion binding	1.71	4,17E-07	7,20E-05
GO:0003723	RNA binding	2.52	1,74E-06	2,02E-04
GO:0008135	translation factor activity, RNA binding	3.99	3,51E-05	2,93E-04
GO:0016874	ligase activity	3.22	4,51E-05	3,47E-04
GO:0008168	methyltransferase activity	2.77	1,22E-04	6,93E-04
GO:0003735	structural constituent of ribosome	3.04	2,15E-04	1,04E-03
GO:0008092	cytoskeletal protein binding	2.55	2,47E-04	1,05E-03
GO:0016791	phosphatase activity	2.57	5,25E-04	1,98E-03
GO:0005198	structural molecule activity	2.43	1,41E-03	4,79E-03
GO:0003924	GTPase activity	2.64	3,52E-03	1,01E-02
GO:0016491	oxidoreductase activity	1.72	3,56E-03	1,01E-02
GO:0016853	isomerase activity	1.91	1,32E-02	3,45E-02
GO:0008233	peptidase activity	1.47	3,79E-02	9,21E-02

Table 11. GO term enrichment analysis for upregulated proteins in *fac*-$[Re(CO)_3(CTZ)(tmp)(PF_6)$ treated parasites.

Biological Process				
ID	Name	Fold enrichment	P-value	Bonferroni
GO:0007010	cytoskeleton organization	6.16	1,01E-03	3,14E-02
GO:0065003	protein-containing complex assembly	3.61	5,75E-03	8,91E-02
GO:0048856	anatomical structure development	7.39	2,75E-02	1,96E-01
GO:0005975	carbohydrate metabolic process	2.5	3,17E-02	1,96E-01
GO:0016071	mRNA metabolic process	2.96	4,46E-02	2,30E-01
Molecular Function				
GO:0008168	methyltransferase activity	2.25	2,52E-02	3,51E-01
GO:0008092	cytoskeletal protein binding	2.24	3,63E-02	3,51E-01

Table S12. Spectral count for the ergosterol synthesis pathway enzymes from *T. cruzi* in both control untreated parasites (C1, C2, and C3) and parasites treated with *fac*-[$Mn(CO)_3(CTZ)(tmp)](PF_6)$ at concentrations corresponding to $5\times EC5_0$ for 4 h (Mn1, Mn2, and Mn3). The measured values for each replicate are reported as spectral counts.

Tritryp ID	ProteinName	Acc. *T. cruzi*	C1	C2	C3	Mn1	Mn2	Mn3
TcCLB.511003.60	acetyl-CoAacetyltransferase, putative	V5BV46	59	65	63	61	48	56
TcCLB.511903.40	3-hydroxy-3-methylglutaryl-CoA synthase, putative	V5B9Q1	224	248	200	315	181	168
TcCLB.506831.40	3-hydroxy-3-methylglutaryl-CoA reductase	V5B780	102	125	115	121	90	93
TcCLB.509237.10	mevalonatekinase, putative	V5BIH8	36	43	37	60	30	32
TcCLB.507913.20	phosphomevalonatekinaseprotein, putative	V5BPT7	15	23	23	17	21	24
TcCLB.511281.40	mevalonate-diphosphatedecarboxylase, putative	V5BEI4	44	46	51	50	37	39
TcCLB.408799.19	isopentenyl-diphosphate delta-isomerase (fragment)	V5BPC4	43	51	44	74	39	42
TcCLB.511823.70	farnesylpyrophosphatesynthase	V5BDA5	37	40	31	46	30	35
TcCLB.507897.20	squalenesynthase	V5D833	8	9	7	--	7	7
TcCLB.503999.10	squalenemonooxygenase, putative	V5BRL1	55	80	48	109	51	59
TcCLB.508175.70	lanosterolsynthase, putative	V5DPI3	52	55	46	41	42	50
TcCLB.506297.260	Lanosterol 14-alpha demethylase	V5C1C6	112	149	125	181	112	140
TcCLB.507969.60	C-14 sterolreductase, putative	V5BKN3	--	--	--	--	--	--
TcCLB.511895.69	C-5 steroldesaturase, putative	V5DER6	--	--	--	5	--	--
TcCLB.509235.20	C-5 steroldesaturase, putative	V5DER6	--	--	--	5	--	--
TcCLB.510873.10	NAD(P)-dependent steroid dehydrogenase protein, putative (fragment)	V5BEU6	40	60	64	57	45	36
lTcCLB.510329.90	C-8 sterolisomerase, putative	--	--	--	--	--	--	--
TcCLB.507853.10	lathosterol oxidase, putative	V5DER6	--	--	--	--	--	--
TcCLB.506945.190	cytochrome p450-like protein, putative	V5BSB7	22	40	33	31	29	24
TcCLB.506577.120	sterol C-24 reductase, putative	V5BPF1	9	14	9	17	13	12